AD-A056 859 YALE UNIV NEW HAVEN CONN DEPT OF ENGINEERING AND AP--ETC F/G 7/4
AN EXPERIMENTAL INVESTIGATION OF THE CRITICAL SUPERSATURATION O--ETC(U)
JAN 78 C F LEE N00014-75-C-0263

UNCLASSIFIED 37 NL

1 OF 1
ADA
056859

END
DATE
FILMED
9-78
DDC

LEVEL II

(11) January 1978 (12) 68 p.

(6) AN EXPERIMENTAL INVESTIGATION OF THE CRITICAL SUPERSATURATION OF FIVE VAPORS IN A SHOCK TUBE,

by

(10) C.F./Lee

(14) 37

(15)

Distribution of this document is unlimited.

Report #37 prepared for Contract N00014-75-C-0263 "Experimental and Theoretical Study of Condensation by Homogeneous Nucleation", (Power Branch, Office of Naval Research, Washington, D.C.). Submitted by Peter P. Wegener, Principal Investigator. Reproduction in whole or in part is permitted for any purpose of the United States Government.

DEPARTMENT OF ENGINEERING
AND APPLIED SCIENCE

YALE UNIVERSITY

CONTENTS

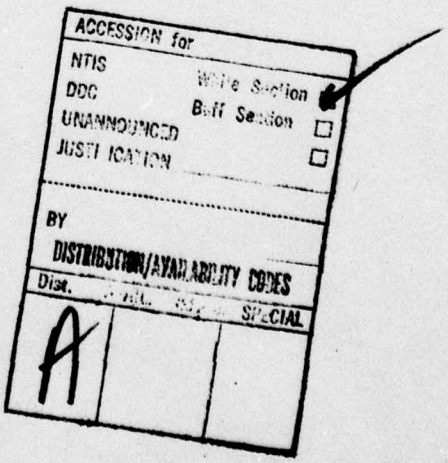

ABSTRACT

Pressure measurements at three different locations in the driver section of a shock tube reveal that the expansion wave generated by diaphragm rupture can be effectively viewed as a simple centered expansion wave whose origin is slightly shifted with respect to the origin of an ideal x-t diagram. The resulting centered expansion wave is used to study the condensation of water, heavy water, benzene, carbon tetrachloride and Freon 11, in an excess of the non-condensing carrier argon. Simultaneous pressure and light scattering measurements determine the onset of condensation. The isentropic flow within the expansion wave is found to be preserved up to the point of the detectable onset of condensation by tailoring the onset conditions to occur at the tail of the expansion wave, thus rendering a simple analysis of the experiments possible.

The experimental onset conditions of the various substances studied generally agree with previous findings in supersonic nozzles, shock tubes and diffusion cloud chambers. No difference is found in the onset of condensation of H_2O and D_2O. The homogeneous nucleation of both H_2O and D_2O is well predicted by the classical theory if it is assumed that both vapors nucleated as supercooled liquid droplets at 17-44°C and 18-49°C below their respective melting points. The homogeneous nucleation of benzene at 47-73°C below its melting point also follows the classical theory if solid condensates are assumed. Agreement with the classical theory is also found for carbon tetrachloride. The nucleation rates of Freon 11 are found to be higher than those predicted by the classical theory.

1. Introduction

Vapor condensation can occur either by heterogeneous nucleation, i.e., a near equilibrium condensation on foreign nuclei, or by homogeneous (and binary) nucleation which takes place on condensation nuclei which are spontaneously produced by fluctuation in the supersaturated vapor (or vapors) itself, at conditions removed from equilibrium. Although condensation phenomena commonly found in nature or encountered in technology usually take place by heterogeneous nucleation, the study of homogeneous nucleation is of fundamental importance to our understanding of all condensation processes. Moreover, homogeneous (and binary) nucleation is of direct interest in many branches of science and technology, e.g. atmospheric physics, steam turbines, MHD-processes, nuclear and high energy physics tools, isotope separation,etc. Unfortunately, despite over fifty years of intensive theoretical and experimental research, a fully satisfactory theory of homogeneous nucleation is still not available, primarily owing to our imperfect understanding of the liquid state. Following the discovery of a thermodynamic criterion for phase instability (Thomson, 1870; Helmholtz, 1886; Gibbs, 1878), Volmer and Weber (1926) initiated a quantitative treatment of the kinetics of condensation which was later developed by others (e.g. Becker and Döring, 1935; Volmer, 1939; Zeldovich, 1942; Frenkel, 1946). This led to the so-called classical (liquid drop) theory of homogeneous nucleation which aims to predict the steady state nucleation rate in terms of the free energy of formation of the critical cluster (McDonald,

1962, 1963; Abraham, 1974). The free energy of formation of the critical cluster (or liquid drop) is evaluated in terms of the macroscopic surface free energy (or surface tension) of the bulk condensate and its volume free energy. In so far as the critical clusters (in situations of high supersaturations) usually contain a few molecules and have sizes of about 10Å (or less), it is doubtful that macroscopic thermodynamic properties such as surface tension can be applied to them. Moreover, these clusters, like larger molecules, are capable of Brownian motion, which could contribute significantly to their free energies. The importance of properly accounting for the translational and rotational motion in the free energy of formation of these clusters has long been recognized (Frenkel, 1946; Rodebush, 1949; Kuhrt, 1952). A recent controversy arising out of the statistical mechanical derivation of the theory centers around different views on the structure of the cluster and in particular, on the varying degrees of resemblance of cluster and bulk condensate (Kuhrt, 1952; Lothe and Pound, 1962, 1969; Dunning, 1965, 1969; Reiss and Katz, 1967; Reiss, 1970). These differing views predict nucleation rates that are different by a magnitude drastically exceeding experimental uncertainties. While the work of Kuhrt, Dunning and Reiss essentially restores the classical theory, Lothe and Pound's theory yields a nucleation rate which is 10^{17} to 10^{20} times larger than that predicted by the classical theory for common substances. It is interesting to note that existing data from various experimental methods on the critical supersaturations of many substances seem to support the classical theory (Volmer

and Flood, 1934; Scharrer, 1939; Wegener and Wu, 1976; Katz et al., 1975, 1976). The glaring exceptions are the nozzle experiments of Dawson et al. (1969) and Jaeger et al. (1969) for the organic vapors benzene, Freon 11, ammonia and chloroform which were said to exhibit much higher nucleation rates tending to support the Lothe and Pound theory. However, there are serious uncertainties associated with these experiments stemming from possible heterogeneous or binary nucleation due to vapor contamination and inappropriate choice of property-values for the condensate (Wu, 1972; Katz et al.,1976). Furthermore, the recent diffusion cloud chamber results of Katz et al. (1975, 1976) showed that the homogeneous nucleation of chloroform, Freon 11 and benzene were all in agreement with the classical theory. In view of such controversies in theory and experiment, it is felt that more reliable experimental data are needed to test the proposed theories and to cast new light on the whole matter.

The oldest experimental tool for studying homogeneous nucleation is the expansion cloud chamber invented by Wilson (1897). It utilizes the transient expansion caused by a rapid withdrawal motion of the piston to achieve supersaturation of the vapor. By repeated expansions to successively higher values of supersaturation until a visible fog appears, a critical supersaturation can be determined. This technique was used in early condensation research on a number of substances by Powell (1928), Volmer and Flood (1934), Scharrer (1939) and many others (see e.g. Das Gupta and Ghosh, 1946). Although qualitative agreement with the classical theory was obtained,

quantitative evaluation of the data is often elusive owing to the complexity of the process involved. Recently, Kassner and his co-workers have carefully studied these problems and have made many improvements (Allard and Kassner, 1965; Kassner and Schmitt, 1966; Allen and Kassner, 1969). Their measurements on the nucleation rate of water (the only substance they studied) in a helium atmosphere agree reasonably well with the classical theory.

More recently, a diffusion cloud chamber has been used to study condensation by homogeneous nucleation (Langsdorf, 1952; Franck and Hertz, 1956; Katz and Ostermier, 1967; Katz, 1970; Katz et al., 1975, 1976). By boiling the vapor from a liquid pool and condensing it on a cooled upper plate, a steady upward thermal diffusion current is established, thus the difficulties of unsteady operation in an expansion cloud chamber are avoided. A light noncondensing carrier gas, such as helium or hydrogen, is used so that the gas density will decrease with height, thus maintaining stability by preventing convection currents. The temperature (T) and the partial pressure (p_v) of the condensing vapor decrease approximately linearly with increasing height while the equilibrium pressure (p_∞), having an approximately exponential dependence on temperature, decreases more rapidly with increasing height. Thus the supersaturation (p_v/p_∞) is unity at top and bottom surfaces and is greater than unity in between, reaching its maximum value near the top surface. When the pool and upper plate temperatures are adjusted properly, condensation becomes visible at a particular altitude as drops begin to rain back into

the pool. The state of the vapor at this location is found by solving the combined heat and mass transport equations for the mixture of vapor and inert gas. Although the diffusion cloud chamber has now emerged as a powerful tool for studying nucleation (largely due to the efforts of Reiss and of Katz and their co-workers), it has several major limitations. The solution of the transport equations requires a precise knowledge of the boundary conditions (e.g. temperatures at the boiling and condensing surfaces) and the transport coefficients of the gaseous mixture. While the former is difficult to measure precisely, the latter is only relatively well known for a limited number of substances. Moreover the substances studied must be liquid at both the top and bottom plates. This restricts nucleation measurements to temperatures below the critical point and above the triple point. There are also other practical difficulties. For example, in Katz's apparatus, he found that in order to avoid convection currents a pressure ratio (defined as total pressure divided by the vapor pressure at the liquid pool surface) of larger than 2 to 3 has to be employed. Since his chamber consists of a glass ring sealed by rubber gaskets, the range of his experimental temperatures and pressures is narrow, especially for substances having high vapor pressures at their triple points. For these reasons, he was not able to study ammonia and was able to study benzene at only one temperature (Katz et al., 1975).

The supersonic nozzle, introduced by Oswatitsch (1941, 1942) in condensation research, is one of the most useful tools for studying condensation, mainly because its steady state

experimental environment is well understood and easily controlled. Its application has already been well summarized in the literature (Stodola, 1927; Stever, 1958; Wegener and Mack, 1958; Wegener and Pouring, 1964; Wegener, 1969; Wegener and Wu, 1977). However, the nozzle has its limitations as well. Owing to the large mass flow rates involved, it is not suited to handle rare, expensive gases or toxic gases. Precooling or preheating is difficult. Moreover, because of the high cooling rates in nozzle expansions, the question often arises if the steady-state nucleation rate can be established in the short time available. The induction times (i.e. the times required for the establishment of the steady state nucleation rate) have been estimated to be of the order of a few microseconds (see e.g. Andres and Boudart, 1965; Courtney, 1962). With the exception of the high intensity molecular beams in the hole-type nozzle expansions[*], the time of persistence of the supersaturated state in a typical converging-diverging nozzle appears to be significantly longer than the induction time and experimental evidence exists that steady state nucleation prevails (see e.g. Wegener and Pouring, 1964; Wegener and Wu, 1977).

The shock tube[**], in contrast, combines many desirable properties of the cloud chamber and the supersonic nozzle. Like the supersonic nozzle, its operation is well understood

---

[*] The cooling rate in a molecular beam experiment is typically 10^9 °C/s (Gallagher and Fenn, 1974) as compared with 10^6 °C/s in a typical nozzle experiment (Wegener and Pouring, 1964).

[**] The operation of a shock tube is described in Chapter 2.

in terms of one dimensional gasdynamics (Glass and Hall, 1959). Permitting batch experiments like the cloud chamber, it has the advantage of providing accurately controlled experimental conditions and easy exchange of test substances. Only small amounts of test vapors are required which can be prepared with great care, thus toxic as well as costly substances can be studied. The wholly confined system can be thoroughly cleaned by pumping it to a high vacuum prior to an experiment. This greatly reduces the problem of vapor contamination which might lead to heterogeneous or binary nucleation. Since the flow history as observed at a fixed location is different depending on its distance from the diaphragm location, the shock tube offers the possibility of studying the effects of cooling rate on the condensation process. By making observations at different locations along the driver section one can cover, in a single experiment, a range of cooling rates extending from those of cloud chambers (10^2 °C/s) to those of the nozzle (10^6 °C/s). With appropriate cooling or heating facilities, a wide range of substances may be investigated over a wide range of experimental conditions.

The shock tube was first applied to condensation studies by Wegener and Lundquist (1951) who employed the rapid cooling capabilities of the unsteady expansion wave in the driver section to achieve condensation of H_2O by homogeneous nucleation. Glass and Patterson (1955) provided the first streak photographs showing the condensation zone in the expansion wave. The first series of condensation experiments on different vapors in the shock tube were attempted by Courtney (1965) who studied the

condensation of H_2O, CH_3OH and CCl_4 using static pressure and light scattering measurements at four different locations. However the uncertainties of the flow conditions in his experiments precluded the determination of onset conditions from his data. Since then there have been various applications of different parts of the shock tube flow to condensation studies. For example, Homer (1971, 1972) utilized the constant thermodynamic environment behind the incident shock wave to study the nucleation and growth of lead particles. Kung and Bauer (1971) investigated the nucleation of iron vapor with the so-called tailored-interface technique which exploited the expansion fan produced as a result of the interaction between the contact surface and the reflected shock wave. Unfortunately, the gasdynamics of these complex flows are difficult to characterize accurately, thus rendering it difficult to obtain reliable nucleation rate data from these experiments.

In this work, the unsteady isentropic expansion wave is chosen as the technique for studying vapor condensation because of its simple flow structure as well as its close analogy to the already well-known steady isentropic expansion in the nozzle. Recently, the unsteady expansion wave has also been applied by others to condensation studies. Kawada and Mori (1973) used it to study the nucleation and growth rates of several refrigerant vapors by simultaneously measuring the static pressure, gas density (by a Mach-Zehnder interferometer) and light absorption. They defined the onset of condensation as the point where the transmitted light has been attenuated by 5%. Barrand and Rieutord (1973) studied the condensation

of water vapor in argon and helium by static pressure measurements at four locations in the driver section. Using light scattering and pressure measurements, Barschdorff (1975) investigated the carrier gas effects on the homogeneous nucleation of water vapor. Most recently, Glass et al. (1977) studied the condensation of water vapor in an unsteady expansion wave using pressure measurements and density measurements by both laser Fabry-Perot interferometry as well as differential interferometry.

This work begins with a review of our understanding of the gasdynamics of the simple centered expansion wave (Chapter 2). Experimental investigation of the real expansion wave reveals that it can be well described by the equations for a simple centered wave if a virtual origin is found for it (Chapter 3). Next, it is experimentally shown that heat addition effects are avoided if the tail of the expansion wave is adjusted to meet the condensation onset locus at the observation station. Thus the onset conditions can be measured unambiguously (Chapter 4). Rayleigh light scattering is again shown to be a reliable tool for detecting the onset of condensation (Appendix 3), especially for low latent heat substances. The critical supersaturations of five different vapors (H_2O, D_2O, C_6H_6, CCl_3F) are determined with simultaneous pressure and light scattering measurements (Chapter 5). The results are compared with theory in Chapter 6 and the conclusions are summarized in Chapter 7.

In summary, the new contributions of this work are believed to be the following:

(1) Static pressure measurements at three different locations in the driver section of a shock tube show that the real expansion wave generated by diaphragm rupture can be viewed effectively as a simple centered wave with a shifted origin.

(2) Simultaneous pressure and light scattering measurements provide experimental evidence that the isentropic flow in the expansion wave during a condensation experiment is preserved up to the point of condensation onset, if the condensation onset conditions are tailored to occur at the tail of the expansion wave. Thus, complicating heat addition effects due to condensation are avoided and the onset of condensation (i.e. the critical supersaturation) can be accurately determined. This also renders a simple analysis of the experiment possible, allowing the experimental results to be compared with the theory of homogeneous nucleation.

(3) The effects of the purity of water (introduced to produce vapor) on the onset of condensation of its vapor have been experimentally investigated. It is found that the cooling rate in the unsteady expansion wave is sufficiently fast that trace impurities in water, if present, have little effect on the measurable onset of condensation.

(4) New data[a] on the critical supersaturation of five different

[a] With the exception of water, little or insufficient previous work has been done on heavy water (Flood and Tronstad, 1936) and conflicting data exist for the other substances (Jaeger et al., 1969; Dawson et al., 1969; Katz et al., 1975, 1976).

vapors namely, water, heavy water, benzene, carbon tetrachloride and freon-11, have been obtained in the shock tube where the cooling rate ($\sim 10^4$ °C/s) is faster than those of the cloud chamber ($\sim 10^2$ °C/s) and slower than those of the nozzle ($\sim 10^6$ °C/s).

(5) New values of $\bar{r}$ ($\equiv J_{exp}/J_{th}$), the factor by which experiment and classical theory are compared, have been obtained for the five vapors studied.

2. Gasdynamics of the Shock Tube Experiments

The success of applying a flow method to condensation studies depends on the knowledge and control of the gasdynamics of the experimental environment. In the condensation studies described here, the unsteady expansion flow produced in the driver section of a shock tube was used. A shock tube in its simplest form consists of a straight constant-area duct which is divided by a removable diaphragm into a high-pressure driver section and a low-pressure driven section. Under ideal operating conditions*, when the diaphragm is removed, a shock wave rapidly develops and moves into the driven section while a simple isentropic, centered expansion wave is generated and propagates into the driver section (see Figure 2.1). As the shock wave passes through the driven gas, it heats up the driven gas and induces in the latter a drift velocity in the direction of its propagation. The expansion wave cools the driver gas and causes the driver gas to accelerate across it. The condition of the driven gas which is traversed by the shock wave is denoted by 2 ; that of the driver gas traversed by the expansion wave is denoted by 3 ; those of the undisturbed driven and driver gases are denoted by 1 and 4 respectively. The interface between the regions 2 and 3

* (i) the removal of the diaphragm is instantaneous and the gas is set into motion abruptly (i.e. infinite acceleration at time zero);
(ii) there are no three dimensional and viscous effects due to the formation of a wall boundary layer;
(iii) the gases are pure substances in thermodynamic equilibrium everywhere except inside the shock wave.

is known as the contact surface which marks the boundary between the gases that were initially on either side of the diaphragm. The unsteady flows associated with these wave systems are well known (see e.g. Liepmann and Roshko, 1957; Glass and Hall, 1959). Here we shall primarily concern ourselves with the centered expansion wave and the unsteady one dimensional inviscid flow associated with it.

Within such a wave, the flow properties (e.g. fluid velocity, pressure, density, temperature etc.) are constant along one family of the characteristics of the governing differential equations (see e.g. Becker, 1968). In an x-t plane as shown in Figure 2.1, these characteristics* are straight lines, each identified by its constant slope x/t, emanating from a single origin which ideally corresponds to the diaphragm location at time zero.** The slope of each characteristic defines the local wave velocity as

$$c = x/t = u - a \,, \tag{2.1a}$$

where u is the local fluid velocity and a the local sound speed. If the driver gas is a perfect gas (and this is assumed for the following discussion), the local wave velocity can further be expressed as

$$c = \left(\frac{\gamma_4 + 1}{2}\right) u - a_4 \,, \tag{2.1b}$$

* These characteristics are analogous to Mach lines in steady supersonic flow.
** For a list of symbols, see pages vii to ix.

where γ_4 is the ratio of the specific heats in the undisturbed driver gas and a_4 the sound speed in the undisturbed driver gas. At the head of the expansion wave propagating into the driver section, the wave speed is equal to the sound speed in the undisturbed driver gas ahead of it since

$$u = 0 \quad , \qquad c = -a_4 \quad . \tag{2.2a}$$

Within the expansion wave it can be shown (Glass and Hall, 1959) that

$$c = a_4 \left[\frac{2}{\gamma_4 - 1} - \frac{\gamma_4 + 1}{\gamma_4 - 1} \cdot \left(\frac{p}{p_4} \right)^{\frac{\gamma_4 - 1}{2\gamma_4}} \right] , \tag{2.2b}$$

where p is the pressure on the characteristic of slope c. The variation of static pressure with time at x_{obs} is given by

$$\frac{p(t)}{p_4} = \left[\frac{2}{\gamma_4 + 1} - \frac{\gamma_4 - 1}{\gamma_4 + 1} \cdot \left(\frac{x_{obs}}{a_4 t} \right) \right]^{\frac{2\gamma_4}{\gamma_4 - 1}} \quad . \tag{2.3}$$

The other flow variables are related by Poisson's Law,

$$\frac{\rho}{\rho_4} = \left(\frac{p}{p_4} \right)^{\gamma_4} = \left(\frac{T}{T_4} \right)^{\frac{\gamma_4}{\gamma_4 - 1}} = \left(\frac{a}{a_4} \right)^{\frac{2\gamma_4}{\gamma_4 - 1}} \quad , \tag{2.4}$$

since the flow is isentropic.

The local flow velocity can be obtained from Equation (2.1b),

$$u = \frac{dx}{dt} = \left(\frac{2}{\gamma_4 + 1} \right) \cdot \frac{x}{t} + \left(\frac{2}{\gamma_4 + 1} \right) \cdot a_4 \quad . \tag{2.5}$$

Since the flow is unsteady, an observer at a fixed location, x_{obs}, sees with time, different fluid elements which have undergone different flow histories. Thus the variation of a flow variable with time as observed at x_{obs} is, in fact, a succession of instantaneous values taken on by different fluid elements as they flow past this point along different particle paths. The particle path of a fluid element as it traverses the expansion wave can be found by integrating the local fluid velocity in Equation (2.5), thus yielding

$$x(t) = \frac{a_4 t}{(\gamma_4 - 1)} \cdot \left[2 - (\gamma_4 - 1) \cdot \left(\frac{x_o}{a_4 t} \right)^{\frac{\gamma_4 - 1}{\gamma_4 + 1}} \right] , \tag{2.6}$$

where x_o defines the initial position of the fluid element.

By combining the equations of motion of the expansion wave with those of the shock wave, and by matching the boundary conditions ($p_2 = p_3$, $u_2 = u_3$) across the contact surface, we arrive at the basic shock tube operating equation (Liepmann and Roshko, 1957):

$$\frac{p_4}{p_1} = \frac{p_2}{p_1}\left[1 - \frac{(\gamma_4-1)\,(a_1/a_4)\,(p_2/p_1 - 1)}{\sqrt{2\gamma_1}\,\cdot\,\sqrt{2\gamma_1 + (\gamma_1+1)\,(p_2/p_1 - 1)}}\right]^{-\frac{2\gamma_4}{\gamma_4-1}} \quad . \quad (2.7)$$

The expansion strength is given by

$$\frac{p_3}{p_4} = \frac{p_2/p_1}{p_4/p_1} \quad . \quad (2.8)$$

From Equations (2.7) and (2.8), we see that the minimum pressure, p_3, in the expansion wave depends upon the initial diaphragm pressure ratio, p_4/p_1, the initial temperatures T_4 and T_1, the initial ratios of specific heats, γ_1 and γ_4, and the molecular weights, μ_1 and μ_4, of the driven and driver gases through the sound speeds since

$$a_1 = \sqrt{\gamma_1 \frac{R}{\mu_1} T_1} \quad , \quad (2.9a)$$

$$a_4 = \sqrt{\gamma_4 \frac{R}{\mu_4} T_4} \quad . \quad (2.9b)$$

Thus the unsteady flow in the shock tube and in particular, the strength of the expansion wave, p_3/p_4, can be controlled by adjusting the initial conditions of the driver and driven gases. If the other parameters are fixed, as the initial diaphragm pressure ratio, p_4/p_1, is increased, p_3/p_4

decreases, T_3/T_4 decreases, c_3 decreases, u_3 increases and the tail of the expansion fan gradually swings to the right of the x-t diagram. When $c_3 = 0$, the tail of the expansion fan coincides with the vertical t-axis, and the outflow from the driver section is sonic, since $u_3 = a_3$. If p_4/p_1 is further increased, the tail of the expansion fan will be in the driven section and the outflow will be supersonic, since $u_3 > a_3$. Although one can systematically lower p_3/p_4 and T_3/T_4 in the driver section by increasing p_4/p_1, the lowest T_3 and p_3 attainable in the driver section are limited at the conditions of sonic outflow. It can be seen from Equation (2.2b) that when $c_3 = 0$ (sonic outflow),

$$\left(\frac{p_3}{p_4}\right)_{min} = \left(\frac{2}{\gamma_4+1}\right)^{\frac{2\gamma_4}{\gamma_4-1}} \quad , \quad (2.10a)$$

$$\left(\frac{T_3}{T_4}\right)_{min} = \left(\frac{2}{\gamma_4+1}\right)^{2} \quad . \quad (2.10b)$$

Thus, the lowest temperature, $(T_3)_{min}$, which is attainable in the driver section is dependent only on the ratio of the specific heats of the driver gas and the initial driver temperature. For a given T_4, a higher value of γ_4 leads to a lower value of $(T_3)_{min}$. On the other hand, for a given γ_4, a lower value of $(T_3)_{min}$ can be attained only by lowering T_4, i.e. by precooling the driver section.

3. Experiments on the Unsteady Expansion Wave

The heart of the application of the shock tube expansion flow to the condensation studies described here lies in the simple structure of the centered expansion wave. In reality, the flow produced in a shock tube may deviate from that predicted by the simplified ideal theory of Chapter 2 because of the bulging of the diaphragm under pressure, finite diaphragm opening time, finite initial acceleration of the outflow, three dimensional initial flow, wall boundary layer effects, etc. (Glass and Hall, 1959). It is not clear how these departures from ideality may affect the simple structure of the centered expansion wave. Therefore, prior to the condensation study, it was deemed necessary to investigate experimentally the unsteady expansion wave actually produced in the shock tube using dry gases (e.g. argon).

Experiments on the unsteady expansion wave were performed in a three-inch I.D. steel shock tube which was later used for condensation experiments.[a] Initially the whole tube was outgassed for an hour by evacuating it to below 10^{-6} torr with a liquid nitrogen cold-trapped diffusion pump. Next both the driver and driven sections were filled with ultra-high-purity argon gas (obtained from MG Scientific with a rated minimum purity of 99.999%) at different pressures. After recording the initial temperatures and pressures in the two sections, the

[a] Details of the apparatus is given in Appendix 4. The experimental procedure is outlined in Chapter 4.

flow was started by rupturing the diaphragm with a spring-loaded needle. Pressure histories at three different locations situated at 5 inches, 7 inches and 19.5 inches respectively upstream of the diaphragm (i.e. in the driver section), were measured by three calibrated quartz-crystal Kistler Model 606L pressure transducers which were mounted flush with the inner tube wall and electrically insulated from it. The charge outputs from the transducers were converted to amplified voltage signals by Kistler Model 504E Dual Mode Amplifiers and were displayed on the storage screen of a fast single sweep oscilloscope (Tektronix Model 5103N).

This procedure was repeated for many different values of initial diaphragm pressure ratios ranging from $p_4/p_1 = 2.0$ to $p_4/p_1 = 8.0$. The initial temperatures in both sections were kept at ambient temperatures. The initial pressure in the driver section was varied from one to two atmospheres while that in the driven section was varied from 400 to 150 torr. Under these conditions, only relatively weak expansion waves were produced where the outflow from the driver section was subsonic and the terminating characteristics of the expansion waves remained in the driver section. In subsequent condensation experiments (described in Chapter 4), it was found that, in order to avoid complicating heat addition effects due to condensation, it was necessary to terminate the expansion wave in the driver section where the onset of condensation was observed. Therefore, here, we are only concerned with the study of the properties of relatively weak expansion waves where the entire pressure drop occurs in the driver section within a few milliseconds.

Figure 3.1 shows the result of a typical experiment in which the pressure traces measured at three different locations were simultaneously recorded on a single oscillogram. The bottom trace corresponds to the pressure measured at the first observation station (5 inches from the diaphragm location). The top and middle traces correspond to the pressure measurements at the second and third observation stations (7 inches and 19.5 inches from the diaphragm location). The vertical pressure scale is 99 torr/div. for the top and bottom traces and 109 torr/div. for the middle trace. The common time base is 0.5 ms/div. The initial experimental conditions were: p_4 = 777.1 torr, $T_4 = T_1$ = 297.4 K, p_4/p_1 = 3.70. Points of equal pressure can be found at different locations and times. These were mapped into an x-t plane as shown in Figure 3.2. The isobars drawn through these experimental points were found to be straight lines merging at a single point, (+3.0 in, -0.25 ms), not far from the origin of the x-t diagram. This result, seen in Figure 3.2 indicated that viscous effects due to a wall boundary layer were negligible since a boundary layer would give rise to an effectively variable-area duct causing the characteristic to curve. Moreover, the interaction between a wall boundary (laminar or turbulent) and an initially centered wave has been shown to lead to a non-centered wave (Hall et al., 1974). Thus the real expansion wave can be viewed effectively as a simple centered wave with a "virtual" origin which is shifted with respect to the actual diaphragm location. This

fact is further borne out by the remarkable agreement (Figure 3.3) between the wave speeds determined from the slopes of the isobars and the ideal centered-wave theory. However, the virtual origin can be determined best by noting the value of x_{obs} which gives a best fit between the experimentally measured pressure variation, p(t), and the theoretical curve of Equation (2.3). The values of $t_{obs}(=x_{obs}/a_4)$ for each of the three observation stations determined in this manner agreed well with those found from Figure 3.2. Using experimental values of t_{obs}, the pressure measurements from Figure 3.1 can finally be represented by a single curve of p/p_4 versus t/t_{obs} as shown in Figure 3.4.

It is worthy of note that the relatively low initial pressure ratios ($2 < p_4/p_1 < 8$) employed in these experiments produced only weak expansion waves ($0.32 < p_3/p_4 < 0.70$). Therefore the flow occurred at high Reynolds Numbers* (typically 6×10^5) producing only sufficiently thin boundary layers which were not "felt" within measuring accuracy. Under such conditions, the assumption of one dimensional inviscid flow is an excellent one. However, it is well-known that deviation from theory grows with increasing expansion strength, namely low p_3 and Re, which would produce more serious viscous effects arising from thicker boundary layers (Glass

---

* The Reynolds Number here is defined as $Re = \frac{\rho u d}{\eta}$, where ρ = density, u = velocity, η = viscosity and d = hydraulic diameter.

and Hall, 1959). Here, this problem is avoided, and in subsequent condensation experiments under similar conditions, deviations from ideal shock tube operation result primarily from the diaphragm that actually bulges under pressure before rupture, thus physically contributing to a shift of the starting point of the expansion wave to the right in Figure 3.2. Moreover, when the curved diaphragm ruptures, three dimensional effects are introduced in the form of shock wave reflection arising from shock curvature. Shock diffraction and vortices are also produced by the jagged remains of the diaphragm. As a result, the assumption of one dimensional inviscid flow at the origin is not realised. There is also an additional effect causing departure from ideality at the origin. It is recalled that one of the assumptions for ideal operation of a shock tube is infinite acceleration at time zero. Owing to the finite fluid inertia, the initial acceleration will not be infinite, thus the characteristics will not be centered at the origin. Therefore departure from ideality at the origin is associated with the properties of the diaphragm material (i.e. its rupturing characteristics) and the establishment of the initial flow. It was found that close agreement with the ideal centered wave theory was obtained if the diaphragm was loaded near its bursting strength. This can be understood in terms of its shorter opening time and less obstruction to the flow upon rupture, thus approaching the condition of ideal diaphragm removal.

It was found that better agreement with the centered wave theory was obtained at larger distances away from the diaphragm. Because of the extremely short time scales involved at distances

closer to the diaphragm, serious measuring uncertainties arise in determining the virtual origin from a static pressure measurement there. This is in line with previous findings (Courtney, 1965; Barrand and Rieutord, 1973) that the real expansion wave approaches a simple centered wave at a sufficiently large distance from the diaphragm. However, at large distances from the diaphragm, departure from ideality would arise from viscous effects due to the growth of the wall boundary layer which increases with distance from the diaphragm location. Courtney found that it took more than 15 shock-tube diameters (D) for the real expansion wave to fully develop into a centered wave. Barrand and Rieutord found that the expansion wave in a moist gas approached a simple wave when $(x/D) \sim 23$. Here, satisfactory agreement with the simple wave theory was obtained even for $(x/D) \sim 2$. In subsequent condensation experiments, the two observation stations are located at $(x/D)_1 \sim 5.5$ and $(x/D)_2 \sim 10.7$.

In conclusion, the above experiments on the expansion wave indicate that the flow non-idealities in the shock tube can be properly accounted for by determining a virtual origin of the unsteady expansion wave from an actual pressure measurement. This corresponds to a "calibration" of the shock tube expansion flow. The analogy in steady supersonic nozzle flow is the calibration of the nozzle by determining an effective area ratio from an actual static pressure measurement along the length of the nozzle such that boundary layer effects can be properly accounted for.

4. Condensation Experiments

Experiments on the condensation of five different vapors were performed in a three-inch steel shock tube.* The substances studied include: water(H_2O), heavy water(D_2O), benzene(C_6H_6), carbon tetrachloride(CCl_4), and Freon 11 (CCl_3F). Except for some experiments on Freon 11, the condensing vapors are present at low mass fractions in an inert carrier gas.** The carrier gas used in all the condensation experiments is argon since it is known that the nature of the carrier gas plays no important role in the condensation process itself (Barschdorff, 1975).*** In order to ensure that the condensation process studied is due to homogeneous nucleation, it is essential to eliminate all possible sources of contamination which might lead to heterogeneous nucleation or binary nucleation. The three principal sources of contamination are:

(i) impurities in the condensing substance;

(ii) impurities in the carrier gas; and

(iii) impurities in the experimental apparatus.

Therefore the purest commercially available test substances

---

* Details of the experimental apparatus are given in Appendix 4.

** The initial mass fractions, ω_4 (and the initial mole fractions, y_4) of the various substances studied are as follows:

H_2O : $5\times10^{-4} < \omega_4 < 6.5\times10^{-3}$

D_2O : $9\times10^{-4} < \omega_4 < 6.2\times10^{-3}$

C_6H_6 : $0.045 < \omega_4 < 0.145$, $(0.023 < y_4 < 0.080)$

CCl_4 : $0.052 < \omega_4 < 0.168$, $(0.014 < y_4 < 0.050)$

CCl_3F : $0.110 < \omega_4 < 0.456$, $(0.034 < y_4 < 0.196)$

*** Provided that the condensing vapor is present in small mass fractions.

and carrier gas are used. The purity of the test substances and the carrier gas are given in Appendix 1. Since a large amount of the carrier gas is required in each experiment, extra care is taken to further dry and filter the carrier gas (ultra-high-purity argon) to ensure that trace contaminants (particles and vapors) present are reduced to such low levels that they do not interfere with the condensation process studied (see Appendix 1).

In condensation experiments performed in a nozzle, it had been shown theoretically by Oswatitsch (1942) that if the cooling rate is sufficiently high, foreign nuclei, even if present in large numbers are expected to have little effect on the homogeneous nucleation of water vapor in air. Buckle and Pouring (1965) proved this fact experimentally by introducing aerosols (10^6 cm^{-3}!) without affecting the condensation process. Here, the cooling rate ($\sim10^4$ °C/s), though higher than those in the cloud chambers ($<10^2$ °C/s), are smaller than those in the nozzles ($\sim10^6$ °C/s). Moreover, minute concentrations of trace vapor contaminants may produce sufficient foreign nuclei if condensation of the contaminants occurs prior to that of the test vapor or they may interact with the test vapor leading to binary nucleation which often precedes the homogeneous nucleation of either species (Wilemski, 1975; Wegener and Wu, 1976). Thus it was deemed desirable to investigate experimentally the effects of trace impurities present in water on its onset of condensation. Such experiments were performed using water samples of three different purities and the details of these experiments are given in Appendix 2. It was found that the

purity of water had no noticeable effect on its onset of condensation, thus indicating that the unsteady expansion wave was sufficiently rapid that condensation on the trace impurities present were negligible.

The inner surface of the shock tube is thoroughly cleaned with acetone and a sponge to remove any grease, particles and diaphragm fragments present. Prior to an experiment, the whole shock tube is evacuated to below 10^{-6} torr with a liquid-nitrogen-cold-trapped diffusion pump and outgassed for at least an hour (in some cases, overnight). Having taken all these precautions, it is believed that all possible sources of contamination have been eliminated.

The condensing substance, normally in a liquid state, is first injected, by means of a syringe, into an electrically heated vaporising chamber. The test vapor produced is then carefully metered into the shock tube via a needle valve heated by electrical heating tapes. This is to ensure that only the test vapor is introduced, in a controlled manner, into the shock tube. It is found that if the test liquid is accidentally introduced into the system, slow evaporation of the liquid will make the measurement of its partial pressure more difficult and inaccurate. Moreover, if liquid droplets (in the form of an aerosol) are present in the system, they may act as seeds for the condensation process. Once a controlled amount of the test vapor is introduced into the system, its partial pressure is measured with a Statham ±5 psid differential pressure transducer.[a]

[a] See Appendix 4 for details.

The driver tube is next filled with ultra-high-purity argon to a total pressure ranging from 1 to 3 atmospheres. The gas mixture is stirred for 15 minutes by circulation through a sealed Metal Bellows pump. The pressure in the driven section, also filled with argon, is recorded by a Wallace and Tiernan dial gauge with a range from 0 to 800 torr. All pressure gauges were calibrated statically against a precision Wallace and Tiernan Model FA187 mercury manometer which served as a calibrating standard. The temperature in the tube is measured with a calibrated cooper-constantan thermocouple. Five other similar thermocouples distributed along the driver section check the temperature in the tube jacket in order to ensure temperature uniformity. When a steady state of all properties is reached the experiment is started by rupturing the diaphragm with a spring-loaded needle.

Pressure and light scattering measurements are made at two different observations situated at 415 mm (Station 1) and 810 mm (Station 2) upstream from the diaphragm location. Measurements of the static pressure variation with time are made with a Kistler pressure transducer as described in Chapter 3 and Appendix 4. Details of the light scattering measurements are given in Appendices 3 and 4.

The onset of condensation is indicated by a pressure deviation above the pressure for an isentropic expansion. This pressure increase, just as in the steady nozzle flow (Wegener and Pouring, 1964), arises from the release of latent heat to the flow. The simultaneous sharp increase of the light scattering signal due to the sudden appearance of a condensation

aerosol is also noted. In experiments involving low latent heat substances, the pressure deviation is hardly noticeable and onset is indicated only by the sudden "lift-off" of the light scattering signal (see Appendix 3).

The heat addition due to condensation in a subsonic flow generates waves which can propagate both upstream and downstream, thus causing the pressure profile at locations outside the condensation zone to deviate from the isentropic pressure variation. Inside the condensation zone the characteristics become curved due primarily to increasing sound speed caused by heat addition. Shock waves may be produced if these characteristics of the same family intersect. Thus the gasdynamic state at onset at an observation station may be affected by prior condensation elsewhere in the expansion fan. However, if condensation onset, rather than the ensuing droplet growth, etc., is of primary interest, the complication caused by heat addition can be avoided. It is recalled that for a given initial relative humidity, condensation onset occurs at a larger supercooling (i.e., lower temperature) when the cooling rate is higher (Oswatitsch, 1942). Hence close to the origin where the cooling rate is higher, onset occurs close to the tail of the expansion fan, while at a distance infinitely far from the origin onset approaches the saturation characteristic asymptotically (equilibrium condensation). Thus the condensation locus has a curved shape. Recognizing this, Barschdorff (1975) proposed that the initial diaphragm pressure ratio can be adjusted such that the tail of the expansion wave (i.e., the location of the lowest pressure and temperature in the flow field) coincides with the condensation

onset locus at the observation station as shown schematically in Figure 4.1. Since at the observation station there is no influence of prior condensation, the isentropic flow field is preserved up to the point of condensation onset.*

Figure 4.2 provides the experimental evidence of this fortunate state of affairs. A sequence of four consecutive experiments was performed on a given sample of D_2O vapor (p_{v4} = 13.8 torr) in an excess of argon (ω_4 = 0.005). The initial conditions in the driver section were kept approximately constant in all four experiments, while p_1 was systematically increased from 620 torr in Exp 18, to 640 torr in Exp 19, 650 torr in Exp 20, and 660 torr in Exp 21. This is equivalent to squeezing the expansion fan in Figure 4.1 by moving its tail in a counter-clockwise direction, thus pushing the intersection point between the tail of the expansion fan and the condensation onset locus farther away from the origin. Since the initial conditions in the driver section were the same in these experiments, the expansion wave in each experiment was the same except that it was terminated at successively higher pressures. Thus the lowest temperature in the expansion fan, T_3, is changed by 0.5 - 1.5 K in each consecutive experiment. It can be seen that while there was "too much" condensation in Exp 18, there was "none' in Exp 21. Onset of conden-

---

* Possible influence of prior condensation in the uniform flow region between the contact surface and the tail of the expansion wave was found to be negligible as shown in Figure 4.2.

sation was "zeroed in" in Exp. 19 where condensation is seen to be just barely beginning as indicated by the light scattering signal and the pressure bump. Further experimental evidence of the absence of influence of prior condensation is provided by Figure 4.3. Here an onset experiment on H_2O vapor in argon (performed in a manner similar to Exp. 19) is compared with the results of a "dry" expansion with pure argon only under the same experimental conditions. The superimposed pressure traces do not deviate from each other until condensation has just begun. Thus it can be concluded that in such an onset experiment, the isentropic flow field is preserved at the observation station up to the point of condensation onset.

Since the onset conditions are not known beforehand, this iterative procedure is carried out to determine the onset conditions for each given gas mixture.

It is noted that the cooling rates at the first and second observation stations are different by a factor of 2 (see Chapter 4, p.31). Since it is well known that larger cooling rates would lead to larger supercooling and higher critical supersaturation (Oswatitsch, 1942; Smith, 1971), the onset conditions measured at the two observation stations are expected to be different. However, in a single experiment, when the onset conditions at the first station are found at the tail of the expansion wave, the onset conditions at the second station are found to be sufficiently close to the tail of the expansion wave such that heat addition effects due to condensation are negligible. Experimental evidence for this is provided by Figure 4.2 which shows that the onset conditions at both

observation stations can be determined simultaneously in a single experiment.

Except in the case of Freon 11, the initial temperatures in both the driver and driven sections were maintained at ambient temperatures. Owing to the higher vapor pressure of Freon 11, and thus higher initial mass fraction of the condensing vapor, the minimum T_3 obtainable in the driver section is raised because of the decrease in the ratio of the specific heats of the gas mixture as indicated in Equation (2.10b). Therefore, in order to obtain low values of T_3, the driver was precooled to 10-15 °C below the room temperature (~20 °C) with running tap water.

5. Experimental Results

The results of each condensation experiment are in the form of pressure and light scattering signals recorded on an oscillogram. Typical oscillograms from condensation experiments on each of the five substances studied are shown in Figures 5.1 to 5.5. The pressure and light scattering signals from the second observation station are recorded with a 1 ms delay[a] with respect to those from the first observation station. It can be seen from these oscillograms that the onset of condensation is unambiguously identified by the simultaneous appearances of a pressure bump and a sharp rise of the light scattering signal. Just as expected, the "pressure bumps" produced by the relatively low latent heat substances (i.e., C_6H_6, CCl_4, and CCl_3F) are less pronounced than those in the H_2O and D_2O oscillograms. But the onset of condensation for all the substances studied is clearly indicated by the light scattering signal.

The static pressure at onset, p_k, is directly measured from the pressure trace on the oscillogram (see Appendix 4 for details). Since the flow is practically isentropic up to the point of condensation onset, the onset conditions are determined from p_k and the initial conditions simply by

$$p_{vk} = p_k \cdot y_4 = p_k \cdot \left(\frac{p_{v4}}{p_4}\right) , \qquad (5.1)$$

[a] This is achieved with a time delay unit on the recording oscilloscope itself.

and

$$T_k = T_4 \cdot \left(\frac{p_k}{p_4}\right)^{\frac{\gamma_m - 1}{\gamma_m}} , \qquad (5.2)$$

where γ_m is the ratio of the specific heats for the gas mixture given by

$$\gamma_m = \frac{\sum_i y_i C_{pi}}{\sum_i y_i C_{vi}} = \frac{y_4 \cdot \frac{\gamma_v}{\gamma_v - 1} + (1-y_4) \cdot \frac{\gamma_i}{\gamma_i - 1}}{y_4 \cdot \frac{1}{\gamma_v - 1} + (1-y_4) \cdot \frac{1}{\gamma_i - 1}} . \qquad (5.3)$$

The subscripts i, v, and m refer to the inert carrier gas, the condensing vapor and the gas mixture respectively.

The critical supersaturation, S_k, (i.e., the saturation ratio at onset) is calculated from the onset conditions and the vapor pressure of the test substance given in Appendix 1.

$$S_k = \frac{p_{vk}}{p_\infty(T_k)} . \qquad (5.4)$$

In using Equations (5.2) and (5.3) to determine the onset temperature, one assumes that the gas mixture is a thermally and calorically perfect gas. This assumption is considered valid if: (i) condensation takes place in thermodynamic states far removed from the critical point of the condensing vapor; and (ii) the condensing vapor is carried in an excess of a diluent gas which is a perfect gas within the range of experimental conditions (e.g., argon).

While this is definitely the case with water ($\omega_4 < 6.5 \times 10^{-3}$) and heavy water ($\omega_4 < 6.2 \times 10^{-3}$), the experiments on benzene, carbon tetrachloride and Freon 11 must be evaluated in the light of their relatively higher initial mass fractions (especially in the case of Freon 11 where $0.110 < \omega_4 < 0.456$), and the variation of their ratios of the specific heats with temperature as shown in Figure 5.6. It is noted that from a typical initial temperature of 300K to a typical onset temperature around 200K, the values of γ for benzene, carbon tetrachloride and Freon 11 change by 6.7%, 2.2% and 2.6% respectively. Thus it is necessary to investigate the effects of deviation from the calorically perfect gas behavior.

The unsteady expansion wave in a thermally perfect but calorically imperfect gas has been treated by Glass and Hall (1959). The variation of the specific heat of the condensing vapor with temperature can be computed by assuming the molecule to be a harmonic oscillator and rigid rotator and fitting the results with a polynomial (see Appendix 1),

$$\left(\frac{C_p}{R}\right)_v = \sum_{i=0}^{n} a_i T^i \quad , \quad (n = 2) \quad . \tag{5.5}$$

As long as the flow is isentropic, the expansion wave produced is still a simple centered wave. However, the temperature and pressure are now related by:

$$\frac{dp}{p} = \frac{\gamma_m}{\gamma_m - 1} \cdot \frac{dT}{T} = \left(\frac{C_p}{R}\right)_m \cdot \frac{dT}{T} \quad , \tag{5.6}$$

where $$\left(\frac{C_p}{R}\right)_m = \left(\frac{C_p}{R}\right)_i \cdot (1-y_4) + \left(\frac{C_p}{R}\right)_v \cdot y_4 \quad . \tag{5.7}$$

Integrating Equation (5.5) from p_4 to p_k yields

$$\ln\left(\frac{p_k}{p_4}\right) = \left[\left(\frac{C_p}{R}\right)_i \cdot (1-y_4) + a_0 y_4\right] \cdot \ln\left(\frac{T_k}{T_4}\right) + a_1 y_4 \cdot (T_k - T_4) + \frac{a_2 y_4}{2} \cdot (T_k^2 - T_4^2) \quad . \tag{5.8}$$

It is found that for all the experiments on benzene, carbon tetrachloride and Freon 11, the difference between T_k calculated from Equation (5.8) and T_k calculated from Equation (5.2) based on a constant γ_v (at T = 250 K) does not exceed 0.5 K which is well within the current experimental uncertainty of ±1 K. Therefore it can be concluded that the error introduced into T_k by the ideal gas assumption is indeed very small.

The experimental results are summarized and presented in Tables 5.1 to 5.5. The slight difference between the onset conditions measured at the first observation station and those measured at the second observation station could be due to the difference in their cooling rates.

The cooling rate experienced by a fluid element in traversing the expansion fan is given by (Glass and Hall, 1959):

$$\frac{dT}{dt} = -\frac{2T_4}{t} \cdot \frac{\gamma_4 - 1}{\gamma_4 + 1} \cdot \left[N - \frac{2(N+1)}{\gamma_4 + 1}\right]^2 \quad , \tag{5.9}$$

where $N = \frac{x}{a_4 t}$. (5.10)

The cooling rate decreases monotonically from its highest value at the head of the expansion fan to its lowest value at the tail of the expansion. The most appropriate value of dT/dt for characterizing the expansion rate leading to phase change is the average value of dT/dt between $S = 1$ and $S = S_k$. Here the average cooling rates for the first and second observation stations are 2×10^4 °C/s and 1×10^4 °C/s respectively. In the case of Freon 11, owing to the higher initial mass fractions (and hence lower values of γ_m), the average cooling rates for the first and second observation stations are approximately 1×10^4 °C/s and 6×10^3 °C/s. It is recalled that for a given initial relatively humidity, higher cooling rates would lead to larger supercooling and higher critical supersaturation (Oswatitsch, 1942; Smith, 1971; Wegener and Wu, 1977). This fact is clearly borne out by the experimental results presented in Tables 5.1 to 5.5 which show the critical supersaturation measured at station one is consistently higher than that at station two.

The experimental results are finally presented in p versus T plots together with $p_\infty(T)$ of the condensing vapor as shown in Figures 5.7 to 5.10. The results of previous investigators are also shown for comparison. Here we shall merely present the raw data of this work and compare them with data from previous investigation using other experimental techniques (e.g. nozzles, diffusion cloud chambers, shock tubes with

different cooling rates). More detailed discussions of the results will be postponed till the next chapter where the data will be evaluated for comparison with theory.

The experimental results for H_2O and D_2O are shown together in Figure 5.7, which also show previous H_2O data from three different nozzle work (Pouring, 1963; Stein, 1967; Roberts, 1969) and Barschdorff's (1975) shock tube work. We note a partial overlap between this work and Barschdorff's data. In general, the nozzle data lie to the left of this work. This difference is due to the same cooling rate effect mentioned above since the average cooling rates in these different investigations are: 10^6 °C/s (nozzles), 10^5 °C/s (Barschdorff) and 10^4 °C/s (this work). Within the limits of experimental uncertainty, the D_2O data coincide with the H_2O data on the $p - T$ plot. Since the $p_\infty(T)$ of D_2O is lower than that of H_2O, this means that for the same initial partial pressure and temperature, D_2O vapor requires a larger supercooling than H_2O since the isentrope crosses the saturation line at a higher temperature. The same result was found by Flood and Tronstad (1936)* who reported that there was practically no difference in the critical supersaturations of H_2O and D_2O despite the slight differences in their physical properties due to isotopy.

The benzene data are shown in Figure 5.8. The data of Dawson (1967) obtained in a supersonic nozzle and the more recent diffusion cloud chamber data of Katz et al. (1975) are

---

* To the author's knowledge, this is the only previous work on D_2O. See Volmer's book (1939), p.135.

also shown for comparison. The benzene data coincide with Dawson's work despite the fact that the cooling rate here is slower by two orders of magnitude. It is noted that the data of Katz et al. lie approximately 15 °C above the triple point while those of Dawson's and this work are located 48-88 °C and 67-73 °C respectively below the triple point.

The carbon tetrachloride data are shown in Figure 5.9 together with Barschdorff's shock tube data (1972) and Katz et al.'s diffusion cloud chamber data (1976). The experimental results lie slightly to the right of Barschdorff's data. Just as before, this is rationalized on the basis of their different cooling rates of 10^4 °C/s (this work) and 10^5 °C/s (Barschdorff). Just as in the case of benzene, the onset points are found to lie 19.7-42.2 °C below the melting point (250.53 K) whereas Katz et al's data lie well above the melting point.

The Freon 11 data are shown in Figure 5.10 together with Dawson et al.'s supersonic nozzle data (1969) and Katz et al.'s diffusion cloud chamber data (1976). The results partially coincide with Katz et al.'s data and lie well above the melting point of 162.04 K. In the experiment involving lower initial mass fractions of Freon 11, the light scattering signal shows oscillatory behavior at onset making it difficult to determine the onset point accurately. Therefore the onset points in these experiments are determined only by the "pressure bumps" which can be more easily identified (see Exp. 84 in Figure 5.5).

6. Comparison of Results with Theory

Theoretical Prediction of Onset

We now turn to the comparison of the experimental results with the theory of homogeneous nucleation. The approach

adopted here is analogous to the treatment of steady condensing flows in a supersonic nozzle first proposed by Oswatitsch (1942). In order to use the nucleation theory to predict the measurable onset of condensation, one needs to evaluate the mass fraction of the condensate, g, accumulated along a particle path finally reaching the experimentally determined point of condensation onset. The problem is formulated by combining the equations of motion, an equation of state and expressions for homogeneous nucleation rates and droplet growth laws (Wu, 1977). This leads to a system of integro-differential equations similar to those originally derived by Oswatitsch for nozzle flows. This method of data evaluation has been previously used by Barschdorff (1975). Different numerical schemes for solving these equations are discussed in detail in the literature (Wegener and Mack, 1958; Gyarmathy and Meyer, 1965; Hill, 1966; Jaeger et al., 1969; Dawson et al., 1969; Wegener, 1969; Wu, 1974) and they need not be repeated here. However, those aspects of this formulation which are relevant to this work dealing in contrast with unsteady isentropic flow will be briefly discussed below.

Since the effects of heat addition due to phase change are negligible prior to the onset of condensation, the gasdynamic problem is simplified to one of isentropic flow[4] (see Chapter 2). Once a virtual origin of the unsteady expansion

[4] An elegant treatment including nucleation, droplet growth and heat addition in rarefaction waves is given by Sislian and Glass (1976).

wave is deduced from an actual measurement of the static pressure variation (see Chapter 3) during a condensation experiment, the entire flow field in the expansion fan prior to condensation onset is uniquely defined. The onset of condensation is determined by noting the time when the pressure deviation from an isentropic expansion is detected, or when the light scattering signal first appears. The particle path passing through the experimental onset point is found from Equation (2.6) (see Figure 4.1).

The condensing vapor contained in a fluid element travelling along this particle path becomes supersaturated on crossing the saturation characteristic in the expansion fan. Droplets of critical size, r^*, as given by the Gibbs-Thomson Equation

$$r^* = \frac{2\sigma u_v}{\rho_c RT \ln(p_v/p_\infty)} \quad , \qquad (6.1)$$

are produced at a rate given by a certain homogeneous nucleation rate expression (to be discussed shortly).

The growth of these surviving droplets in a supersaturated environment is governed by the rate of vapor deposition on the droplet surface as well as the rate of heat conduction from the droplet to the surrounding gas.

By combining the Fick's law of diffusion and the Fourier's law of heat conduction, Gyarmathy (1963) derived an expression for the growth rate of a spherical droplet in a continuum*

---

* Here a continuum is defined as a gaseous medium where the

environment of arbitrary supersaturation and composition. He extended the validity of his formula to transitional and free molecular flow regimes by invoking a correction factor which is a function of the Knudsen number. The general form of his growth law can be written as

$$\frac{dr}{dt} = \frac{1}{\rho_\ell r} \cdot \frac{(1-r^*/r)}{(1+\theta\ Kn)} \cdot \left[\frac{L^2 \mu_v}{\lambda RT^2} + \frac{p-p_v}{p} \cdot \frac{RT}{p\, D u_v} \right]^{-1} \cdot \ln S \quad , \qquad (6.2)$$

$$\text{where} \quad \theta = \frac{2\sqrt{2\pi}}{\xi} \cdot \frac{\gamma}{\gamma+1} \cdot \frac{1}{1.5\ Pr} \quad , \qquad (6.3)$$

ξ = thermal accommodation coefficient,

Pr = Prandtl number = $\frac{\overline{\eta C}_p}{\lambda}$

The two terms in the square brackets represent the thermal and the diffusional resistances to droplet growth. In general, the thermal resistance is much larger than the diffusional resistance* and the droplet growth rate is dominated by the

---

(cont'd)
Knudsen number is much less than unity. The Knudsen number is defined as

$$Kn = \bar{l}/r$$

where $\bar{l}$ is the mean free path of the surrounding gas and r the characteristic length (e.g. droplet radius).

* Gyarmathy (1963) showed that in the case of a water droplet growing in moist air, the thermal resistance is an order of magnitude larger than the diffusional term.

rate of heat transport away from the droplet.

However, if the droplet size remains much smaller than the mean free path of the surrounding gas, (i.e. Kn >> 1) throughout the entire period of growth, it is more convenient to use the free molecular growth law as derived by Wu (1972) based on well-known results from kinetic theory

$$\frac{dr}{dt} = \alpha' \cdot \frac{m_c}{\rho_c} \cdot \frac{p_v}{\sqrt{2\pi m_c kT}} \quad , \tag{6.4}$$

where α' is the effective condensation coefficient that formally accounts for evaporation. In the experiments in this work, the droplet and the surrounding gas are nearly in thermal equilibrium owing to the abundance of the carrier gas present and the low latent heats of some of the condensing substance (e.g. CCl_4 and CCl_3F). An expression for α' for the near isothermal condition was first given by Wu (1972) as

$$\alpha' = \frac{\alpha \left[1 - p_r(T)/p_v\right]}{1 + \frac{\alpha}{K_v} \cdot \frac{P_r(T)}{P_v} \cdot \frac{L\, m_c}{kT} \cdot \frac{L\, m_c/kT - 1/2}{1 + \left(\frac{K_i\, m_c}{K_v\, m_i}\right) \cdot \left(\frac{P_i}{P_v}\right) \cdot \sqrt{\frac{m_c}{m_i}}}} \quad , \tag{6.5}$$

where α is the mass accommodation coefficient, $p_r(T)$ is the radius-dependent saturation vapor pressure obtained by rearranging Equation (6.1), and $K = (\gamma+1) / 2(\gamma-1)$. The mass ($\alpha$) and thermal ($\xi$) accommodation coefficients are assumed to be

equal to unity. The validity of this assumption has been verified by experiments (Mills and Seban, 1967; Bonacci et al., 1976; Wachman, 1962).

The remaining uncertainty in solving the system of equations lies in the choice of a proper theory to describe the physics of nucleation. In contrast to droplet growth laws which are thought to be well understood, the current controversy over the validity of the various physical models proposed for the nucleation rate equation is still unresolved as discussed e.g. by Dunning (1969), Lothe and Pound (1969), Wegener and Parlange (1970), Reiss (1970) and others. Hence it is useful to introduce an empirical adjustment factor Γ (Barschdorff et al., 1972; Wegener and Wu, 1977) such that

$$J_{exp} = \Gamma \cdot J_{th} \tag{6.6}$$

where J_{exp} is the nucleation rate which correctly matches an experiment, and J_{th} a nucleation rate expression chosen from any of the existing theories of homogeneous nucleation. Here we choose the classical theory, developed by Becker and Doring (1935), Volmer (1939), and Frenkel (1946) and others*, as the basis for comparison since it is found to give remarkable qualitative agreement with many substances (e.g. Katz et al., 1975, 1976; Wegener and Wu, 1977). A convenient form for this steady-state nucleation rate is given by Volmer's Equation

---

* All these authors obtained essentially the same result (Yang, 1963; Wegener and Pouring, 1964).

(Volmer, 1939), which is expressed in cgs units as follows (e.g. Wegener, 1969):

$$J_{th} \equiv J_{cl} = 5.4 \times 10^{19} \left(\frac{p_v}{T}\right)^2 \cdot \frac{(\sigma \mu_v)^{\frac{1}{2}}}{\rho_c} \cdot \exp\left[-17.6 \left(\frac{\sigma}{T}\right)^3 \cdot \left(\frac{\mu_v}{\rho_c}\right) \cdot \frac{1}{(\ln S)^2} \right] \quad (6.7)$$

The complete flow equations (i.e. the equations of motion, of nucleation and of droplet growth) can now be solved simultaneously on a digital computer. The value of Γ is found in an iterative manner. In each successive calculation for a fixed experimental environment, Γ is systematically varied until the theoretical prediction matches with the thermodynamic states observed at the experimental onset point. Agreement of theory and experiment is forced when the mass fraction of the condensate has a value $10^{-4} < g < 10^{-3}$, since this condition is found to correspond to the instance when the pressure deviation from the isentropic value is detected or when the scattered light is first observed in the case of H_2O.* In view of the uncertainties in theory and experiment lumped together, general agreement with the classical theory of homogeneous nucleation appears to be indicated if $10^{-3} < \Gamma < 10^{3}$.

In those experiments where onset of condensation is

* For the low latent heat substances studied here, the corresponding values of g at onset is $10^{-3} < g < 10^{-2}$ for approximately 1% pressure deviation from the isentropic value.

observed at temperatures below the melting point, it is unclear whether the condensate is nucleated as supercooled liquid droplets or as solid particles (crystalline or amorphous). Condensation onset at states below the melting point was observed for all the substances studied except for Freon 11 as shown in the last columns in Tables 5.1 to 5.5. As indicated in Equation (6.7), the nucleation rate is strongly dependent on the supersaturation of the vapor and the physical properties of the condensate. At a given temperature, the exponential factor in the nucleation rate equation has essentially the following form:

$$J_{cl} \sim \exp\left[- \text{constant} \cdot \frac{\sigma^3}{(\ln S)^2} \right] \quad (6.8)$$

Thus J_{cl} is extremely sensitive to σ and $\ln S$. In evaluating a given experiment, a large σ will lead to a low J_{cl}, thus a large Γ whereas a low p_∞ will lead to a large supersaturation, thus a low Γ. Therefore, in the Γ-calculations, an increase in σ and a decrease in p_∞ have a counteracting influence on Γ. Since the σ and p_∞ are distinctly different for solid and liquid, in those experiments where onset of condensation was observed at states below the melting point, the results must be evaluated for both cases of solid and liquid condensates.

Condensation of Water and Heavy Water

The results of a typical Γ-calculation for a water condensation experiment are shown in Figure 6.1. The various

profiles shown are calculated along a particle path passing through the experimental onset point at station one (virtual x_{obs} = 521 mm, t = 2.64ms). The value of Γ is adjusted to 10^5 to yield g = 1.31×10^{-4} at the onset point. The curves of S and log J are seen to peak steeply at onset. In the 100μs period immediately preceding onset, N rises from 5.26×10^6 to 1.61×10^{10} and g increases even more sharply from 5.81×10^{-9} to 1.31×10^{-4}. These calculated profiles confirm the notion of a "critical" supersaturation at onset. The mass average droplet radius grows from r^* (∿10Å) to approximately 160Å at onset, thus confirming the validity of applying free molecular growth law in this case.

Similar results are obtained for D_2O experiments. The results of both calculations are summarized and presented in Table 6.1. In the case of supercooled liquid H_2O, the calculations yield low values of Γ (∿10^3 to 10^5) which are in agreement with the results of previous investigations as shown in Table 6.2. Low values of Γ (∿10^1 to 10^3) are also found for supercooled liquid D_2O. Of all the physical properties which affect the nucleation rate (Equation (6.7)), the vapor pressures of H_2O and D_2O are visibly different as shown in Figure 5.7 while their surface tensions* are almost

---

* Except for water, the supercooled liquid σ_ℓ of the other substances studied are obtained by extrapolation from the normal liquid σ_ℓ to temperatures below the melting point (see Appendix 1) while their σ_s values are estimated from (Dunning, 1976)

$$\frac{\sigma_s}{\sigma_\ell} = \frac{L_s}{L_\ell} \cdot \left(\frac{\rho_s}{\rho_\ell}\right)^{2/3} .$$

the same (see Appendix 1). However, as seen in Figure 5.7, the experimental scatter of the onset data of H_2O and D_2O is roughly the same as the difference between their vapor pressure curves. Thus, in view of the current measuring uncertainties of ΔT_k = ±1 K which lead to $\Delta(\log \Gamma)$ = ±2, no difference can be discerned in the homogeneous nucleation of H_2O and D_2O if the condensate is assumed to be supercooled liquid droplets.

In the case of solid condensates, higher values of Γ are found for both H_2O ($\Gamma \sim 10^{12}$ to 10^{14}) and D_2O ($\Gamma \sim 10^8$ to 10^{12}). The solid H_2O results contrast sharply with the relatively low Γ-values (10^5 to 10^7) reported by Wegener and Wu (1977). Here the large Γ-values are due to the large increase in σ_s (96 erg/cm²) as compared to σ_ℓ (79.3 erg/cm²) while the corresponding decrease in $p_{\infty,s}$ is insufficient at this temperature range (∿ 245 K) to offset the surface energy effect. At lower temperatures, the $p_{\infty,s}$ curve falls off more rapidly than the extrapolated curve of $p_{\infty,\ell}$, thus producing a much larger supersaturation effect. Meanwhile the difference between σ_s and σ_ℓ has narrowed since the value of σ_s is taken as constant while the extrapolated σ_ℓ increases with decreasing temperature (see Appendix 1). This explains the lower Γ-values found by Wegener and Wu (1977) for Stein's nozzle experiments where onset occurred at a lower temperature (∿ 220 K). The higher Γ-values found

---

(cont'd)
The σ_ℓ of supercooled water has been measured (Hacker, 1951) and σ_s of ice has been estimated by McDonald (1953) to be 96 erg/cm².

for solid D_2O can also be rationalized in the same manner, i.e. a larger supersaturation effect due to the lower $p_{\infty,s}$ of D_2O. Again, no significant difference is found for the Γ-values of solid H_2O and solid D_2O.

It is often stated that water can be supercooled to as low as -42 °C before crystallization commences (Mason, 1957). In view of the fact that, here, the onset of condensation of H_2O is observed at temperatures only 17-43 °C below the melting point (0 °C), it is unlikely that the condensate in these experiments is solid although direct and convinsing experimental evidence (e.g. infra-red absorption of the droplets, low energy electron diffraction, etc.) is needed to confirm this. If we assume liquid condensates, the low Γ-values (for supercooled liquid) found for H_2O and D_2O indicate that the onset of condensation of these substances are well predicted by the classical theory of homogeneous nucleation.

Condensation of Benzene, Carbon Tetrachloride and Freon-11

As noted before, the lower latent heats (L) of benzene, carbon tetrachloride and Freon 11 as compared to those of H_2O and D_2O, lead to smaller pressure deviations and higher values of g (10^{-3} to 10^{-2}) at the measurable onset of condensation.* This also affects the choice of an appropriate growth law for the theoretical prediction of onset of condensation. It is recalled that the droplet growth rate, as given by Equation (6.2),

* This range of values of g corresponds to approximately 1% pressure deviation from the isentropic pressure.

is dominated by the thermal resistance term which depends on L^2. Thus a lower L will give rise to a much larger dr/dt since the amount of heat to be conducted away from the droplet is reduced. At typical onset conditions, dr/dt for benzene, carbon tetrachloride and Freon 11 is roughly an order of magnitude larger than that for water and heavy water ($dr/dt \simeq 5 \times 10^{-2}$ cm/s). Here the droplets grow rapidly from r^* ($\sim$ 10-15Å) to sizes ($\sim$ 2000Å) larger than the mean free path of the surrounding gas (i.e. $Kn \gg 1$). Since the flow behavior with respect to the droplet changes from the initial free molecular regime to the transitional regime, and finally to the continuum regime, Gyarmathy's more versatile growth law is used instead of Wu's strictly free molecular growth law.

The calculation of Γ for the experiments on benzene, carbon tetrachloride and Freon 11 are carried out in the same manner as water and heavy water. The results are summarized and presented in Table 6.1. The effect of larger dr/dt is clearly manifested in the larger $\bar{r}$ ($\sim$ 1000-3000Å) and smaller N ($\sim 10^7$ cm^{-3}) calculated at onset as compared to those found for water and heavy water.

Since the onset of condensation of benzene is observed at temperatures 47-73 °C below its melting point (278.67 K), the question again arises as to whether the condensate is supercooled liquid or solid. Again, the experiments have to be evaluated for both cases, just as in the case of H_2O and D_2O. As shown in Table 6.1, low values of Γ (10^1 to 10^3) are found for the case of solid condensate which is expected

to be the stable phase at these low temperatures. On the other hand, if one assumes that the condensate remains as a supercooled liquid at these temperatures, higher values of Γ (10^7 to 10^8) are found. These results seem to confirm the experiments of Dawson et al.(1969) as shown in Table 6.3. However, the high Γ-values found for the liquid condensate here are at odds with the recent diffusion cloud chamber data of Katz et al.(1975) which show that at temperatures well above the melting point, the homogeneous nucleation of benzene follows the classical theory. Since the normal liquid properties are better known than those of either supercooled liquid or solid, it is far more desirable to observe onset of condensation at temperatures above the melting point. The next logical step for us to take is to extend the range of observation to higher temperatures (e.g. by raising the initial temperature, T_4). This will reveal any trend in the variation of Γ (if there is a solid-liquid transition in the condensate) leading to a more meaningful interpretation of the data.

In the case of carbon tetrachloride, onset of condensation is again observed at 20° to 42°C below the melting point (250.53K). Here, besides the question of whether the condensate is supercooled liquid or solid, an additional uncertainty arises as to what solid properties to use in the Γ-calculations since it is known that three solid phases can exist in this temperature range of 208 to 231K (Rudman and Post, 1966; Koga and Morrison, 1975; Morrison and Richards,

1976). Between the melting point and the solid-solid phase transition at 225.7 K, a face-centered cubic phase (Ia) and a rhombohedral phase (Ib) are possible. Below the transition temperature of 225.7 K, a third solid, a monoclinic phase (II), is the most stable phase. However, in view of the recent findings of Badiali et al. (1976) that (i) between 250.53 K and 225.7 K, the Ib phase is the most stable phase, and (ii) the Ib phase can be supercooled to 200 K, the properties of the Ib phase (see Appendix 1) are used for the solid Γ-calculations here.

The calculations yield low values of Γ for both the solid (10^2 to 10^4) and the liquid (10^5 to 10^6). The latter result is in agreement with the Γ-values found for Barschdorff's (1972) experiments in the same shock tube with a higher cooling rate of 10^5 °C/s (see Figure 5.9 and Table 6.2). Thus, despite the poorly known property values of the solid and supercooled liquid phases, the onset of condensation of carbon tetrachloride is found to be well predicted by the classical theory of homogeneous nucleation. This conclusion is in line with Katz et al.'s (1976) recent diffusion cloud chamber data which show that the critical supersaturation of carbon tetrachloride measured at temperatures well above the melting point agrees well with the classical theory.

The Freon 11 experiments provide the only case in this work where the onset of condensation occurs well above the melting point. Hence the uncertainty regarding the state of the condensate is eliminated. In the previous work on Freon 11 (Dawson et al., 1969), a serious uncertainty was associated

with the possible seeding of the Freon 11 vapor due to the 35ppm of H_2O present in the carrier air as shown by the seeding calculation of Wu (1972). Here, this uncertainty is eliminated since the carrier argon contains less than 1ppm of H_2O and the Freon 11 vapor used contains less than 10ppm of H_2O. However, the calculations yield Γ-values (10^9 to 10^{12}) which are only slightly lower than those found for Dawson et al.'s (1969) experiments ($\Gamma \sim 10^{12}$ to 10^{14}) as shown in Table 6.2. Provided that no experimental errors exist, the high Γ-values found for freon-11 suggest that the nucleation rates of Freon 11 are higher than those predicted by the classical theory. This result is at odds with the recent diffusion cloud chamber of Katz et al. (1976) which showed that the condensation of Freon 11 followed the classical theory. Since the impurities in both the condensing vapor and the non-condensing carrier gas have been reduced to such low levels as mentioned above, it is unlikely that binary or heterogeneous nucleation could account for this discrepancy, although a direct experimental investigation of the binary nucleation of the Freon 11/water system is needed to confirm this.

7. Summary and Conclusions

The critical supersaturation of five different vapors was experimentally investigated using the unsteady expansion wave in the driver section of the shock tube. Using pure argon, the real expansion wave produced was experimentally investigated by simultaneous pressure measurements at three different locations in the driver section. An experimental x-t diagram showed that the real expansion wave retained the simple structure of the ideal expansion wave fan but with a shifted origin. It was found that deviations from ideal shock tube operation, arising mainly from the non-ideal rupture of the initially curved diaphragm and the establishment of the initial flow, can be accounted for by defining a virtual origin from the pressure measurement at a single location. Thus the gasdynamics associated with the real expansion wave can be well characterized by the ideal theory of a simple, centered expansion wave with a shifted origin. It was experimentally shown that during a "moist" expansion, the isentropic flow in the unsteady expansion wave is preserved up to the point of measurable onset of condensation if the locus of condensation onset is adjusted to intersect the tail of the expansion wave at the observation station. Thus complicated heat addition effects due to condensation are avoided and the thermodynamic states at onset, i.e. critical supersaturation, can be easily measured with confidence.

Rayleigh scattering of laser light at 90° was used as a diagnostic tool for detecting the sudden appearance of a

condensed phase at onset. The light scattering technique was shown to be as reliable as the measurement of pressure deviation at the onset of condensation for high latent heat substances like water and heavy water (see Appendix 3). In the case of low latent heat substances where the pressure deviations are less noticeable, the light scattering technique proved to be a valuable tool.

New data on the critical supersaturation of the following substances were obtained:

(1) water, H_2O;

(2) heavy water, D_2O;

(3) benzene, C_6H_6;

(4) carbon tetrachloride, CCl_4

(5) Freon 11, CCl_3F.

The following conclusions can be drawn from this work:

(1) The cooling rate attainable in the unsteady expansion wave was found to be sufficiently rapid that trace impurities in water if present, has no noticeable effect on the measurable onset of condensation of its vapor.

(2) The condensation of water and heavy water, assuming supercooled liquid condensate was nucleated, followed the classical theory of homogeneous nucleation.

(3) Within the limits of current measuring accuracies, no difference in the onset of condensation of water and heavy water was found despite slight differences in their physical properties due to isotopy.

(4) The onset of condensation of benzene was well predicted by the classical theory if the solid clusters were nucleated at 47-73 ^{o}C below its melting point.

(5) The onset of condensation of carbon tetrachloride was well predicted by the classical theory.

(6) The nucleation rates of Freon 11 were found to be higher than those predicted by the classical theory.

REFERENCES

Abraham, F.F. (1974) Homogeneous Nucleation Theory (Academic Press, N.Y.)

Allard, E.F. and Kassner, J.L., Jr. (1965) J. Chem. Phys., 42, 1401.

Allen, L.B. and Kassner, J.L., Jr., (1969) J. Colloid Interface Sci., 30, 81.

Andres, R.P. and Boudart, M. (1965) J. Chem. Phys., 42, 2057.

ASHRAE (1966) Guide and Data Book, Fundamentals and Equipment, 1965, 1966 (Ashrae, N.Y.).

Badiali, J.P., Bruneaux-Poulle, J., Defrain, A. (1976) J. Ch m, Phys., 73, 113.

Barrand, J.P. and Rieutord, E. (1973) Int. J. Heat Mass Transfer, 16, 101.

Barschdorff, D. (1971) Forsch. Ing.-Wes., 37, 146.

Barschdorff, D., Dunning, W.J., Wegener, P.P. and Wu, B.J.C. (1972) Nature (Phy. Sci.), 240, 166.

Barschdorff, D. (1972) Private communications.

Barschdorff, D. (1975) Phys. Fluids, 18, 85, 529.

Bartholomé, E. and Clusius, K. (1935) Z. physik. Chem., B28, 175.

Becker, E. (1968) Gas Dynamics (Academic Press, N.Y.)

Becker, R. and Döring, W. (1935) Ann. Phys., 24, 719.

Binnie, A.M. and Green, J.R. (1943) Proc. Roy. Soc. (London), A181, 134.

Bonacci, J.C., Myers, A.L., Monghri, G. and Eagleton, L.C. (1976) Chem. Eng. Sci., 31, 609.

Bridgman, P.W. (1931) The Physics of High Pressure (Bell and Sons), Dover Reprint, 1970.

Bridgman, P.W. (1935) J. Chem. Phys., 3, 597.

Buckle, E.R. and Pouring, A.A. (1965) Nature, 208, 367.

Clumpner, J.A. (1970) Condensation of ethyl alcohol by homogeneous nucleation in a supersonic nozzle. Ph.D. Thesis, Yale Univ., New Haven, Conn.

Clumpner, J.A. (1971) J. Chem. Phys., 55, 80[illegible].

Cockett, A.H. and Ferguson, A. (1939) Phil. Mag., 885.

Courtney, W.G. (1962) J. Chem. Phys., 36, 2018.

Courtney, W.G. (1965) Condensation in a Rarefraction Wave. Technical Report Supplement No. 2 Submitted to Office of Naval Research under Contract NOnr 4154(00) Dec. 1965. Available from National Technical Information Service, Springfield, Va., Accession No. AD-625667.

CRC Handbook of Chemistry and Physics (1972-73) (Chemical Rubber Publ. Co., Cleveland, Ohio) 53rd Edition.

Das Gupta, N.N. and Ghosh, S.K. (1946) Rev. Mod. Phys., 18(2), 225.

Dawson, D.B. 1967) Condensation of supersaturated organic vapors in a supersonic nozzle. Gas Turbine Laboratory Report #90, Mass. Inst. of Tech., Cambridge, Mass.

Dawson, D.B., Wilson, E.J., Hill, P.G. and Russell, K.C. (1969) J. Chem. Phys., 51, 5389.

Deych, M. Ye., Saltanov, G.A., Stephnchuk, V.F. and Orlova, V.M. (1969) Heat Transfer-Soviet Research, 1, #2, 135.

Dunning, W.J. (1969) in The Physical Chemistry of Aerosols, A General Discussion of the Faraday Society (The Univ. Press, Aberdeen).

Dunning, W.J. (1964) in Heterogeneous Combustion, 15, Progress in Aeron. and Astronaut., H.G. Wolfhard et al., eds. (Academic Press, N.Y.)

Dunning, W.J. (1965) Adsorption et Croissance Cristalline, Colloques Internationaux du C.N.R.S., Paris (1965) 369.

Dunning, W.J. (1969) Chap.1 in Nucleation, A.C. Zettlemoyer, ed. (Marcel Dekker, N.Y.)

Dunning, W.J. (1976) Private communications.

Dupont (1965) Thermodynamic Properties of Freon-11, E.I. Dupont de Nemours, Organic Chemicals Dept., Wilmington, Delaware.

Eisenberg, D. and Kauzman, W. (1969) The Structure and Properties of Water (Ozford Univ. Press, N.Y.)

Fletcher, N.H. (1970) The Chemical Physics of Ice (Cambridge Univ. Press, Cambridge).

Flood, H. and Tronstad, L. (1936) Z. physik. Chem., A175, 347.

Franck, J.P. and Hertz, H.G. (1956) Z. Physik, 143, 559.

Frenkel, J. (1946) Kinetic Theory of Liquids (Oxford Univ. Press, N.Y.)

Gallagher, R.J. and Fenn, J.B. (1974) J. Chem. Phys., 60, 3492.

Gay, R. and Lemanceau, B. (1956) Cahiers de Phys., 70.

Gibbs, J.W. (1878) Collected Works (Longmans, Green, N.Y., 1928).

Glass, I.I. and Hall, J.G. (1959) Handbook of Supersonic Aerodynamics, Section 18, Shock Tubes. NAVARD Report 1488, Vol.6 (A Bureau of Naval Weapons Publication).

Glass, I.I. and Patterson, G.N. (1955) J. Aero. Sci., 22, #2, 73.

Glass, I.I., Kalra, S.P. and Sislian, J.P. (1977) AIAA Journal, 15, #5, 686.

Gyarmathy, G. (1963) ZAMP, 14, 280.

Gyarmathy, G. and Meyer, H. (1965) Spontane Kondensation. VDI-Forschungsheft 508 (VDI-Verlag GMbH Düsseldorf).

Hacker, P.T. (1951) NACA Tech. Note 2510, NACA, Washington.

Hales, J.L. (1970) J. Physics E: Sci. Instr., 3, 855.

Hall, J.G., Srinivasan, G. and Rathi, J.S. (1974) AIAA Journal, 12, #5, 724.

Head, R.M. (1949) Investigation of spontaneous condensation phenomena. Ph.D. Thesis, Cal. Inst. of Tech., Pasadena, Ca.

Helmholtz, R. (1886) Ann. Physik, 27, 508.

Hill, P.G. (1966) J. Fluid Mech., 25, 593.

Homer, J.B. (1971) in Shock Tube Research, J.L. Stollery, A.G. Gaydon and P.R. Owen, eds. (Chapman and Hall, London) Paper #62.

Homer, J.B. and Hurle, I.R. (1971) Proc. Roy. Soc. (London), A327, 61.

International Critical Tables (1929) Vol. 5 (National Research Council, McGraw Hill).

Jackowski, A.W. (1974) J. Chem. Thermodyn., 6, 49.

Jaeger, H.L. (1966) Condensation of supersaturated ammonia and water vapor in supersonic nozzles. Master's Thesis, Mass. Inst. of Tech., Cambridge, Mass.

Jaeger, H.L., Willson, E.J., Hill, P.G. and Russell, K.C. (1969) J. Chem. Phys., 51, 5380.

JANAF Thermochemical Tables (1971) U.S. Dept. of Commerce, NSRDS-NBS. (US) 37.

Jasper, J.J. (1972) J. Phys. Chem. Ref. Data, 1, 859.

Jones, W. (1968) J. Chem. Phys., 48, 207.

Jordan, T.E. (1954) Vapor Pressure of Organic Compounds (Interscience, N.Y.).

Kassner, J.L., Jr. and Schmitt, R.J. (1966) J. Chem. Phys., 44, 4166.

Katz, J.L. (1970) J. Chem. Phys., 52, #6, 4733.

Katz, J.L. and Ostermier, B.J. (1967) J. Chem. Phys., 47, 478.

Katz, J.L., Scoppa, C.J., II, Kumar, N.G. and Mirabel, P. (1975) J. Chem. Phys., 62, #2, 448.

Katz, J.L., Mirabel, P., Scoppa, C.J., II and Virkler, T.L. (1976) J. Chem. Phys., 65, #1, 382.

Kawada, H. and Mori, Y. (1973) Bulletin of the JSME, 16, #97, 1053.

Keenan, J.H. and Keyes, F.G. (1936) Thermodynamic Properties of Steam (Wiley, N.Y.)

Kell, G.S. (1967) J. Chem. Eng. Data, 12, 66.

Kerker, M. (1969) The Scattering of Light and other Electromagnetic Radiation (Academic Press, N.Y.)

Kiss, I., Jákly, G. and Illy, Mrs. H. (1966) Acta Chimica Acad. Sci. Hung., 47, 379.

Koga, Y. and Morrison, J.A. (1975) J. Chem. Phys., 62, #8, 3359.

Kuhrt, F. (1952) Z. Physik, 131, 185, 205.

Kung, R.T.V. and Bauer, S.H. (1971) in Shock Tube Research, J.L. Stollery, A.G. Gaydon and P.R. Owen, eds. (Chapman and Hall, London) Paper #61.

Langsdorf, A. (1952) Ind. Eng. Chem., 44, 1928.

Liepmann, H.W. and Roshko, A. (1957) Elements of Gasdynamics (Wiley, N.Y.).

Lothe, J. and Pound, G.M. (1962) J. Chem. Phys., 36, 2080.

Lothe, J. and Pound, G.M. (1969) in Nucleation, A.C. Zettlemoyer, ed. (Marcel Dekker, N.Y.)

McDonald, J.E. (1953) J. Meteorol., 10, 416.

McDonald, J.E. (1962) Am. J. Phys., 30, 870.

McDonald, J.E. (1963) Am. J. Phys., 31, 31.

Mallinckrodt AR Laboratory Chemicals and Plastics Catalog (1973) St. Louis, Missouri.

Mason, B.J. (1957) The Physics of Clouds (Oxford Univ. Press, London).

Matheson Gas Data Book (1971) Matheson Gas Products, New Jersey.

Mie, G. (1908) Ann. Physik, 25, 377.

Miller, G.A. (1962) J. Chem. Eng. Data, 7, 353.

Mills, A.F. and Seban, R.A. (1967) Int. J. Heat Mass Transfer, 10, 1815.

Morrison, J.A. and Richards, E.L. (1976) J. Chem. Thermodyn., 8, 1033.

Oswatitsch, K. (1941) Jahrb, Duetsch. Luftfahrtforsch., 1, 703.

Oswatitsch, K. (1942) ZAMM, 22, 1.

Pouring, A.A. (1963) An experimental and analytical investigation of the homogeneous nucleation from the vapor phase. Ph.D. Thesis, Yale Univ., New Haven, Conn.

Powell, C.F. (1928) Proc. Roy. Soc. (London), A119, 553.

Rayleigh, Lord (1881) Phil. Mag., 12, 81.

Reid, R.C. and Sherwood, T.K. (1966) The Properties of Gases and Liquids (McGraw-Hill, N.Y.).

Reiss, H. (1970) J. Statistical Phys., 2, 83.

Reiss, H. and Katz, J.L. (1967) J. Chem. Phys., 47, 2202.

Roberts, R. (1969) A Light Scattering Investigation of Droplet Growth in Nozzle Condensation. Gas Turbine Laboratory, Report #97, Mass. Inst. of Tech., Cambridge, Mass.

Rodebush, W.H. (1949) Chem. Rev., 44, 269.

Rudman, R. and Post, B. (1966) Science, 154 (3752), 1009.

Scharrer, L. (1939) Ann. Physik, 35, 619.

Shimanouchi, T. (1972) Tables of Molecular Vibrational Frequencies, Consolidated Volume I. NSRDS-NBS (US) 39 (U.S. Dept. of Commerce).

Sislian, J.P. and Glass, I.I., (1976) AIAA Journal, 14, 1731.

Smith, L.T. (1971) AIAA Journal, 9, #10, 2035.

Stein, G.D. (1967) Condensation of ice clusters by homogeneous nucleation from the vapor phase. Ph.D. Thesis, Yale Univ., New Haven, Conn.

Stein, G.D. (1969) J. Chem. Phys., 51, 938.

Stever, H.G. (1958) in Fundamentals of Gas Dynamics, Vol. III (Princeton Univ. Press, Princeton, N.J.)

Stodola, A. (1927) Steam and Gas Turbines (McGraw Hill, N.Y.)

Sverdlov, L.M., Kovner, M.A. and Krainov, E.P. (1974) Vibrational Spectra of Polyatomic Molecules (Wiley, N.Y.).

Svoboda, V., Veselý, F. Holub, R. and Pick, J. (1973) Collect. Czechoslov. Chem. Commun., 38, 3539.

Thomson, W. (1870) Proc. Roy. Soc. (Edinburgh), 7, 63.

Timmermans, J. (1965) Physico-chemical constants of pure organic compound (Elsevier, N.Y.)

Van de Hulst, H.C. (1957) Light Scattering by Small Particles (Wiley, N.Y.).

Volmer, M. (1939) Kinetik der Phasenbildung (Steinkopff, Dresden and Leipzig).

Volmer, M. and Flood, H. (1934) Z. physik. Chem. (Leipzig), A170, 273.

Volmer, M. and Weber, A. (1926) Z. physik. Chem. (Leipzig), 119, 277.

Wachman, H.Y. (1962) ARS Journal, 32, 2.

Wegener, P.P. (1969) in Nonequilibrium Flows, Part I, Vol.1 of Gasdynamics, P.P. Wegener, ed. (Marcel Dekker, N.Y.)

Wegener, P.P. and Lundquist, G. (1951) J. Appl. Phys., 22, #2, 233.

Wegener, P.P. and Mack, L.M. (1958) in Advances in Applied Mechanics, Vol.5, H.L. Dryden and T. von Karman, eds. (Academic Press, N.Y.)

Wegener, P.P. and Parlange, J.-Y. (1970) Naturwiss., 57, 525.

Wegener, P.P. and Pouring, A.A. (1964) Phys. Fluids, 7, #3, 352.

Wegener, P.P. and Stein, G.D. (1969) Twelfth Symposium (International) on Combustion, 1183.

Wegener, P.P. and Wu, B.J.C. (1976) in Precipitation, Faraday Discussion, #61.

Wegener, P.P. and Wu, B.J.C. (1977) in Nucleation Phenomena, A.C. Zettlemoyer, ed. (Elsevier Scientific Co., Amsterdam).

Wilemski, G. (1975) J. Chem. Phys., 62, #9, 3763.

Wilson, C.T.R. (1897) Trans. Roy. Soc. (London), A189, 265.

Wu, B.J.C. (1972) A study on vapor condensation by homogeneous nucleation in nozzles. Ph.D. Thesis, Yale Univ., New Haven, Conn.

Wu, B.J.C. (1974) Computer Programs for Calculating Condensation Rate in Steady, Adiabatic Expansions in Supersonic Nozzles. Report #26 for Contract N000 14-67-A-0097-0012. Available from National Technical Information Service, Springfield, Va., Ref. # AD-775257.

Wu, B.J.C. (1977) Analysis of Condensation in the Centered Expansion Wave in a Shock Tube. Paper presented at the ASME Symposium on Condensing High Speed Flows, in New Haven, Conn.

Yang, W.T. (1963) A study of homogeneous nucleation from vapor to droplets. Ph.D. Thesis, Yale Univ., New Haven, Conn.

Zeldovich, Y.B. (1942) J. Exp. Theor. Phys. (U.S.S.R.), 12, 525.

Appendix 1. Selected Physical and Thermodynamic Properties of Test Substances and Carrier Gas

Several physical and thermodynamic properties of the test substances and the carrier gas are needed in the data reduction procedures outlined in Chapters 5 and 6. This appendix lists the numerical values and the temperature dependent properties used in this work. The purity of the test substances studied and the carrier gas used are also given in this appendix.

Unless otherwise indicated, the units of the various property values are as follows: p_∞ , vapor pressure in atm; T , temperature in degrees K; ρ , density in g cm^{-3}; σ , surface tension in dyne cm^{-1}, or surface free energy in erg cm^{-2}; L , latent heat of vaporization in cal g^{-1}; n_D , refractive index for sodium light (λ = 5893 Å). The subscripts s , ℓ , and ∞ refer to the solid state, the liquid state, and flat surface bulk values respectively. The sources of these literature values are quoted in parentheses following each property.

(1) Water, H_2O

Molecular Weight = 18.016

Ice I-liquid-vapor triple point = 273.16 K

Melting point = 273.15 K

Boiling point = 373.15 K

(Eisenberg & Kauzmann, 1969)

Ratio of specific heats, γ = 1.325

Vapor Pressure:

$$\text{Liquid,}\quad \log \frac{p_c}{p_{\infty,\ell}} = \frac{x}{T}\left[\frac{a'+b'x+c'x^3}{1+d'x}\right], \qquad \text{(A1.1)}$$

where p_c = 218.167 atm,

T_c = 647.27,

$x = T_c - T$,

a' = 3.2437814,

b' = 5.86826×10^{-3},

c' = 1.1702379×10^{-8},

d' = 2.1878462×10^{-3}. (Keenan & Keyes,1936)

$$\text{Solid,}\quad \log p_{\infty,s} = 7.582 - \frac{2676}{T}. \qquad \text{(A1.2) (Wegener,1969)}$$

Density:

$$\text{Liquid,}\quad \rho_\ell = \frac{\sum_{n=0}^{5} a_n (T-273.15)^n}{1 + b_1 (T-273.15)}, \qquad \text{(A1.3)}$$

where a_0 = 0.9998396,

a_1 = 18.224944×10^{-3},

a_2 = -7.922210×10^{-6},

a_3 = -55.44846×10^{-9},

a_4 = 149.7562×10^{-12},

a_5 = $-393.2952 \times 10^{-15}$,

b_1 = 18.159725×10^{-3}. (Kell,1967)

Solid, ρ_s = 0.92 (A1.4) (McDonald,1953; Eisenberg & Kauzmann,1969)

Surface Tension:

Liquid, $\sigma_\ell = 75.83 - 0.1477(T-273.16)$ (A1.5) (Jasper,1972)

Solid, σ_s = 96.0 (A1.6) (Fletcher,1970)

Heat of Vaporization:

Liquid, $L_\ell = 595.38 - 0.5577(T-273.15)$ (A1.7) (Int.Crit.Tables,1929)

Solid, $L_s = 677.28 - 0.0292(T-273.15)$ (A1.8) (Int.Crit.Tables,1929)

Refractive Index:

Water, n_D^{20} = 1.33299 (A1.9) (CRC Handbook,1972-73)

Ice, n_D = 1.3104 (A1.10) (CRC Handbook,1972-73)

(2) Heavy Water (Deuterium Oxide), D_2O

Molecular Weight = 20.031

Ice I-liquid-vapor triple point = 276.98 K

Melting point = 276.97 K (Eisenberg & Kauzmann,1969)

Boiling point = 374.59 K

Ratio of specific heats, γ = 1.325

Vapor Pressure:

$$\text{Liquid,}\quad \ln\left[\frac{p_{\infty,\ell}(H_2O)}{p_{\infty,\ell}(D_2O)}\right] = -\frac{70.87}{T} + \frac{33630}{T^2} \qquad \text{(A1.11) (Jones,1968)}$$

Solid, $\log p_{=,s} = -\frac{2767.1}{T} + 7.806$ (A.12)
(Kiss et al. 1966)

Density:

Liquid, $\rho_\ell = \frac{\sum_{n=0}^{4} a_n (T-273.15)^n}{1 + b_1 (T-273.15)}$, (A.13)

where $a_0 = 1.104690$,
$a_1 = 20.09315 \times 10^{-3}$,
$a_2 = -9.24227 \times 10^{-6}$,
$a_3 = -55.9509 \times 10^{-9}$,
$a_4 = 79.9512 \times 10^{-12}$,
$b_1 = 17.96190 \times 10^{-3}$. (Kell, 1967)

Solid, $\rho_s = 1.0165$ (A.14) (Bridgman,1935)

Surface Tension:

Liquid, $\sigma_\ell = 75.17 - 0.1723(T-273.15)$ (A1.15)
(Cockett & Ferguson,1939)

Solid, $\sigma_s = 95.0$ (A1.16)
(Estimated from latent heat*)

---

* In the absence of any experimental measurements, a crude estimate of the surface free energy of a solid can be obtained by applying the following formula (Dunning,1976):

$$\frac{\sigma_s}{\sigma_\ell} = \frac{L_s}{L_\ell} \cdot \left(\frac{\rho_s}{\rho_\ell}\right)^{2/3} \quad \text{(A1.17)}$$

This formula estimates the surface free energies of H_2O and D_2O to be 81.5 erg cm^{-2} and 80.7 erg cm^{-2} respectively. However, McDonald (1953), using a more elaborate method of estimating σ_s (by considering the cleavage work of an ice crystal) produced a value of 96 erg cm^{-2}. Since McDonald's value for σ_s (H_2O) is considered more reliable than that calculated from Equation (A1.17), the value of $\sigma_s(D_2O)$ used here was calculated

Heat of Vaporization:

Liquid, $L_\ell = 589.35 - 0.5577(T-273.15) + \frac{6671.94}{T}$ (A1.18)
(Jones,1968)

Solid, $L_s = 630.57$ (A1.19)
(Bartholomé & Clusius,1935)

Refractive Index:

Liquid, $n_D^{20} = 1.33044$ (A1.20)
(CRC Handbook,1972-73)

(3) Benzene, C_6H_6

Molecular Weight = 78.108

Triple point = 5.524°C
Melting point = 5.5165°C (Timmermans,1965)
Boiling point = 80.10°C

Vapor heat capacity at constant pressure*,

$C_p/R = 1.265894 + 1.863579\times10^{-2}T + 3.418677\times10^{-5}T^2$ (A1.21)

(cont'd)
as follows:

$\sigma_s(D_2O) = \left(96 \times \frac{80.7}{81.5}\right) = 95.1$ erg cm^{-2}

For the other test substances (i.e. C_6H_6, CCl_4, CCl_3F), the values of σ_s were calculated from Equation (A1.17).

* Ideal-gas heat capacities of the vapor are computed from a knowledge of its molecular structure and all its vibrational frequencies (JANAF,1971; Shimanouchi,1972; Sverdlov et al., 1974), assuming the molecule to be a rigid rotator and a simple harmonic oscillator (Reid & Sherwood,1958). The computed values are then fitted with a polynomial and the values of γ are computed from

$$\gamma = \frac{C_p/R}{C_p/R - 1}$$

Ratio of specific heats, $\gamma = \frac{C_p/R}{C_p/R - 1}$

Vapor Pressure:

Liquid, $\log p_{\infty,\ell} = 5.081 - \frac{1785.0}{T}$ (A1.22) (Wegener,1969)

Solid, $\log p_{\infty,s} = 8.0034 - \frac{2836.0}{(T+25.31)}$ (A1.23) (Jackowski,1974)

Density:

Liquid, $\rho_\ell = 0.903074 - 1.13756 \times 10^{-3}(T-273.15)$ (A1.24) (Hales,1970)

Solid, $\rho_s = 1.01456$ (A1.25) (Bridgman,1931)

Surface Tension:

Liquid, $\sigma_\ell = 31.45 - 0.1291(T-273.15)$ (A1.26) (Jasper,1972)

Solid, $\sigma_s = 43.09$ (A1.27) (Estimated from latent heat)

Heat of Vaporization:

Liquid, $L_\ell = \frac{ART(1-Tr)^{0.40}}{Tr}$, (A1.28)

where $A = 9.78055$,

$R = 0.02544$,

$Tr = T/T_{crit}$,

$T_{crit} = 562.09$ K. (Svoboda et al,1973)

Solid, $L_s = 137.31$ (A1.29) (Miller,1962)

Refractive Index:

Liquid, $n_D^{20} = 1.5011$ (A1.30) (Mallinckrodt Catalog,1973)

Solid, $n_D^4 = 1.544$ (a-axis), $= 1.646$ (b-axis), $= 1.550$ (c-axis). (A1.31) (Gay & Lemanceau,1956)

(4) Carbon Tetrachloride (Tetrachloromethane), CCl_4

Molecular Weight = 153.82

Normal boiling point = 349.8 K (Timmermans,1965)

Melting point (Ib → L) = 250.53 K | (Morrison & Richards, 1976)

Transition temperature (II → Ib) = 225.7 K | (Morrison & Richards, 1976)

Vapor heat capacity at constant pressure,

$C_p/R = 2.60804 + 3.6981 \times 10^{-2}T - 4.1374 \times 10^{-5}T^2$ (A1.32)

Ratio of specific heats, $\gamma = \frac{C_p/R}{C_p/R - 1}$

Vapor Pressure (in torr):

Liquid, $\log p_{\infty,\ell} = 6.87926 - \frac{1212.02}{(T-46.74)}$ (A1.33) (Katz et al., 1976)

Solid,

$\log p_{\infty,s} = 8.821 - \frac{1975.3}{T}$, $(225.7<T<250.53)$

$= 9.089 - \frac{2027.0}{T}$, $(T<225.7)$. (A1.34) (Jordan, 1954)

Density:

Liquid, $\rho_\ell = \sum_{n=0}^{3} a_n (T-273.15)^n$, (A1.35)

where $n_0 = 1.63186$,

$n_1 = -1.867 \times 10^{-3}$,

$n_2 = -8.914 \times 10^{-7}$,

$n_3 = 2.943 \times 10^{-9}$. (Katz et al.,1976)

Solid, $\rho_s = 1.788$, (225.7<T<250.53K) | (A1.36) (Rudman & Post,1966)

$= 1.868$, (T<225.7K).

Surface Tension:

Liquid, $\sigma_\ell = 29.49 - 0.1224(T-273.15)$ (A1.37) (Jasper,1972)

Solid, $\sigma_s = 35.398$, (225.7<T<250.53K) | (A1.38) (Estimated from latent heat)

$= 45.77$, (T<225.7K).

Heat of Vaporization:

Liquid, $L_\ell = \sum_{n=0}^{3} a_n (T-273.15)^n$, (A1.39)

where $a_0 = 52.096$,

$a_1 = -6.6999 \times 10^{-2}$,

$a_2 = -6.3305 \times 10^{-5}$,

$a_3 = -4.3574 \times 10^{-7}$. (Int.Crit. Tables,1929)

Solid, $L_s = 58.47$, (225<T<250.53K) | (A1.40) (Morrison & Richards,1976)

$= 65.67$, (T<225.7K).

Refractive Index:

Liquid, $n_D^{15} = 1.4631$ (A1.41) (Timmermans,1965)

(5) **Freon-11 (Trichlorofluoromethane), CCl_3F**

Molecular Weight = 137.38

Boiling point = 296.97 K | (Dupont,1965)

Melting point = 162.04 K

Vapor heat capacity at constant pressure,

$C_p/R = 2.2793 + 0.034546T - 0.35975 \times 10^{-4} T^2$ (A1.42)

Ratio of specific heats, $\gamma = \frac{C_p/R}{C_p/R - 1}$

Vapor Pressure:

Liquid,

$$\log P_{\infty,\ell} = A + \frac{B}{T_R} + C \log T_R + DT_R + \frac{E(F-T_R)}{T_R} \log(F-T_R) ,$$ (A1.43)

where A = 42.14702865,

B = -4344.343807,

C = -12.84596753,

D = 0.004008372507,

E = 0.0313605356,

F = 862.07,

T_R = Temp. in °R = °F + 459.67,

$P_{\infty,\ell}$ = Vapor pressure in psia. (Dupont, 1965)

Density:

Liquid, $\rho_\ell = \sum_{n=0}^{4} a_n T^n$, (A1.44)

where $a_0 = 2.05059$,

$a_1 = -1.34278 \times 10^{-3}$,

$a_2 = -3.81417 \times 10^{-6}$,

$a_3 = 1.10719 \times 10^{-8}$,

$a_4 = -1.62766 \times 10^{-11}$. (Katz et al.,1976)

Surface Tension:

Liquid, $\sigma_\ell = 21.0709 - 0.1261818(T-273.15)$ (A1.45)
(Katz et al.,1976)

Heat of Vaporization:

Liquid, $L_\ell = 46.6 - 0.074(T-273.15)$ (A1.46)
(ASHRAE,1966)

Refractive Index:

Liquid, $n_D^{25} = 1.374$ (A1.47) (Matheson,1971)

(6) Carrier Gas, Argon

Molecular Weight = 39.948

Ratio of specific heats, $\gamma = 1.67$

(7) Purity of the test substances and the carrier gas

The water used in this work was ultra-pure-reagent grade water obtained from the New England Reagent Laboratory, E. Providence, R.I. Distilled water and ordinary New Haven tap water were also used. The effects of the purity of water on the onset of its condensation are discussed in Appendix 2. The heavy water used was manufactured by Thompson Packard (sold exclusively through Wilmad Glass Co. Inc., Buena, N.J.) with a stated minimum isotopic purity of 99.8%. The benzene used was the spectranalyzed AR grade obtained from Fisher Scientific of Fair Lawn, N.J. and contained less than 0.03% of water. The carbon tetrachloride used was SpectrAR (spectrophotometric) grade obtained from Mallinckrodt, St. Louis, Missouri. The Freon-11 used was obtained from Matheson with a stated minimum purity of 99.9% (H_2O < 10ppm). No purification was deemed necessary for any of the test substances since no other impurities were detected by gas chromatography.

The argon carrier gas used was ultra-high-purity grade (rated minimum purity of 99.999%) obtained from MG Scientific Gases. Its principal impurities are listed as : H_2O < 1ppm; O_2 < 1ppm; N_2 < 2ppm; H_2 < 1ppm; THC* as CH_4 < 1ppm. In order to ascertain that these low levels of impurities did not interfere with the nucleation process studied, the ultra-pure-argon was passed through a column of drierite (anhydrous calcium sulfate; dew point = -100°F at 1 atm), followed by a liquid nitrogen cold trap, before entering the shock tube. No

* THC = Total Hydrocarbon Content

discernable effects were found between the condensation experiments performed with this "extra dry" argon and those with the ultra-pure-argon. Subsequently the drying column and the liquid nitrogen cold trap were bypassed. Instead a Matheson Model 450 Purifier was used in conjunction with a replaceable cartridge Model 452 (containing 4A Molecular Sieve) which removed water (dew point = -100°F) and particles over 12 microns.

Appendix 2. Effects of the Purity of Water on the Onset of Condensation of its Vapor

In experimental studies of condensation by homogeneous nucleation using gasdynamic methods, it is often assumed that the cooling rate experienced by the vapor is sufficiently high[a] that effects due to condensation by heterogeneous nucleation on particulates present in the gas and vapor supply may be neglected (Oswatitsch, 1942). This implies that impurities in the condensing vapor would have little effect on the condensation of that vapor (Wegener, 1969). Buckle and Pouring (1965) ascertained experimentally that up to 10^8 particles per cm^3 of foreign nuclei (silver iodide particles 0.1 - 1.0 μm in diameter) had no noticeable effect on the condensation of water vapor in air in a supersonic nozzle. Indeed, it was found that homogeneous nucleation often led to the production of critical nuclei that were more numerous by factors as high as 10^8 than the foreign nuclei present in ordinary laboratory air (Wegener, 1969). However, minute concentrations of trace vapor contaminants may produce sufficient foreign nuclei if condensation of the contaminants occurs prior to that of the test vapor or they may interact with the test vapor leading to binary nucleation which often precedes homogeneous nucleation of either species (Wegener and Wu, 1976; Wilemski, 1975). Thus it was deemed desirable

---

[a] Typical cooling rates are 10^6 °C/s in supersonic nozzles (Stein, 1967) and 10^5 °C/s in this work.

to investigate experimentally the effects of trace impurities in water on the condensation of its vapor.

Water samples of three different purities, ultra-pure reagent grade water, distilled water, and ordinary New Haven tap water were used. The ultra-pure reagent water used (obtained from New England Reagent Laboratory, E. Providence, R.I.) is believed to be the purest commercially available water sample. It is prepared by a comprehensive series of purification processes and analyses which ensure that all contaminants have been removed beyond the limits of clinical measurement. The distilled water used was made with a distillation apparatus in the laboratory. The ordinary New Haven tap water was used without any treatment. The argon carrier gas used was the same ultra-high purity grade that was used in all the other condensation experiments in this work. It is believed that the level of impurities in the carrier gas was so low that it had no effect on the condensation of the test vapor (see Chapter 4).

Figure A2.1 shows the results of the onset experiments performed on the three different water samples with approximately the same initial conditions. Each onset experiment was carried out according to the same experimental procedure outlined in Chapter 4. The results of three such sets of experiments with different initial conditions are shown in Table A2.1. It can be seen that the differences in the onset conditions determined for the three different water samples are insignificant in view of the measuring uncertainties of

$\Delta p_{vk} = \pm 0.4$ torr and $\Delta T_k = \pm 1.0$ K. Figure A2.2 presents the final results together with more onset points from experiments on the ultra-pure reagent grade water. Here the initial and onset conditions of the experiments presented in Table A2.1 are joined by their respective isentropes. It can be concluded that owing to the rapidity of the expansion, the trace impurities in water have no noticeable effect on its condensation onset.

Appendix 3. Details of the Light Scattering Method of Detecting the Onset of Condensation

The term "onset" of condensation is used to denote the observable beginning of the condensation process. In most supersonic nozzle work, this refers to the point where the measured static pressure is first observed to depart from the isentropic value (Oswatitsch, 1942; Head, 1949; Wegener and Pouring, 1964; Jaeger, 1966; Stein, 1967). Detection of onset by pressure measurement depends on the latent heat of the condensing substance. Although substances with a relatively large latent heat[a] generate pronounced pressure deviations at onset, condensation of low latent heat substances lead to pressure deviations that are hardly noticeable. Light scattering provides a more sensitive method of detecting the onset of condensation since it relates directly to the sudden build-up of clusters and their rapidly increasing sizes.

The general case of scattering of a plane polarized, monochromatic electromagnetic wave by a spherical particle was solved by Mie (1908) (e.g. van de Hulst, 1957; Kerker, 1969). Rayleigh (1881) produced a simplified analysis of the problem for the case of small particles when $\frac{2\pi r}{\lambda} << 1$, where r is the particle radius and λ is the wavelength of the light. With gaseous lasers as light sources, Rayleigh

[a] The latent heats of vaporization, in cal/g, of the various test substances at their respective boiling points are: 539.6 (H_2O), 495.4 (D_2O), 94.1 (C_6H_6), 46.4 (CCl_4), 44.8 (CCl_3F).

scattering has been successfully applied to determine the number density and final particle size in supersonic nozzle experiments (Stein, 1969; Wegener and Stein, 1969; Clumpner, 1971). In the present work, the objective is to employ Rayleigh scattering to determine the onset of condensation.

Figure A3.1 shows the schematic arrangement of an observation station[a] situated at 0.810m from the diaphragm location. A Spectra Physics Model 124B 15mW Helium-Neon laser[aa] (λ = 6328 Å) provides a parallel beam of laser light approximately 2.5mm in diameter traversing the centerline of the shock tube. Scattered radiation is detected by a RCA-7265 photomultiplier tube (PMT) looking vertically downward at 90° to the laser beam. The scattering solid angle is defined by the following geometrical parameters: the width(d) of both the window of the PMT housing and the observation window in the shock tube; the distance(S) between them; and the distance(R) from the PMT window to the laser beam. The PMT anode current output is converted to a voltage signal (V_{PMT}) by means of a load resistor (R_L) of 10.12 kΩ. Inserting all the relevant parameters into the Rayleigh scattering equation for single scattering from a monodisperse aerosol, one obtains:

$$\frac{I}{I_o} = \frac{(\pi d^2/4)}{RS} \cdot \left(\frac{2\pi}{\lambda}\right)^4 \cdot \left|\frac{m^2-1}{m^2+2}\right|^2 \cdot Nr^6 \qquad \text{(A3.1)}$$

[a] This has been referred to earlier on in Chapter 4 as the second observation station. The first observation station, situated at 0.415m from the diaphragm location, also has a similar arrangement for light scattering and pressure measurements.

[aa] A Liconix Helium-Cadmium laser was used for some experiments. See Appendix 4 for details.

where m is the refractive index of the scatterer, and I and I_o are the intensities of the scattered radiation at 90° and the incident radiation respectively. The light scattering voltage signal (V_{PMT}) is related to I/I_o as follows:

$$V_{PMT} = \left(\frac{I}{I_o}\right) \cdot I_o \cdot \left(\begin{matrix}\text{Cathode Absolute} \\ \text{Sensitivity}\end{matrix}\right) \cdot \left(\begin{matrix}\text{Current Ampli-} \\ \text{fication Factor}\end{matrix}\right) \cdot R_L \qquad \text{(A3.2)}$$

Given a fixed scattering geometry, a certain laser and PMT, and ignoring the slight variation of the refractive index of the scatterer with temperature, V_{PMT} provides a direct measure of the product Nr^6.

An oscillogram from a typical moist air experiment is shown in the lower left hand corner of Figure A3.2. The onset of condensation occurred at the tail of the expansion fan. The onset conditions were found to be p_{vk} = 5.5 torr, T_k = 245.1 K. The value of Γ (= J_{exp}/J_{cl}) was adjusted to 10^5 to yield $g = 7.5 \times 10^{-4}$ at onset assuming the condensate was in the liquid state. The various profiles of S, $\log J$, r^4, r, N and g can be computed from the measured isentropic pressure distribution only up to the onset point. However, a crude estimate of these profiles beyond onset into the condensation zone is possible if one ignores the small effects of heat addition on the droplet growth process immediately downstream from the onset point while the nucleation rate is set to zero since the slight heating is expected to terminate any further nucleation of new droplets. This assumption is made on the basis of our previous experience with

condensation in nozzle flows, where the nucleation rate is observed to peak sharply near the onset point and decline rapidly once onset has occurred because J has an extremely strong dependence on temperature. Thus once the onset is passed, the pressure is maintained at a constant value (p_3) and the resulting profiles are shown in Figure A3.3 together with the measured isentropic pressure distribution. The S and $\log J$ curves peaked at the same time, approximately 100 μs before the onset point. The minimum of r^4 also occurred at the same time. The curves of N, r and g rose steeply at about the same time. When the measured PMT voltage signal, V_{PMT}, was plotted against these computed values of Nr^6 for the same t, a straight line of unity slope was found on a log-log plot as shown in Figure A3.4, i.e., V_{PMT} varies linearly with Nr^6. This indicated that the light scattering observed was Rayleigh scattering.

A comparison of the measured V_{PMT} with its calculated value based on Equations (A3.1) and (A3.2) is finally presented in Figure A3.2. The lift-off point of the measured V_{PMT} lagged that of the calculated V_{PMT} by 200 μs. However this only translates into the following differences in the onset conditions determined: $\Delta(p_{vk}) = 0.1$ torr, $\Delta(T_k) = 1.4$ K. In light of the uncertainties entering the parameters of the equations used and the crude assumptions made, these discrepancies are insignificant. Thus, it can be concluded that Rayleigh scattering is a reliable method of detecting the onset of condensation.

Appendix 4. Details of the Experimental Apparatus

Shock Tube

A schematic drawing of the 3-inch I.D. steel shock tube is shown in Figure A4.1. It has a driver section of 4.191 m (13.75 feet) and a driven section of 1.219 m (4 feet). The driver section has a jacketed wall which can be filled with circulating hot or cold fluids for either heating or cooling purposes. In addition to the two Welch Duo-Seal mechanical pumps (Model 1397) which independantly pump the driver and driven sections, a 6-inch Norton diffusion pump is connected to the driver section. Thus the whole tube can be evacuated to below 10^{-6} torr.

A stainless steel welded bellows pump (Model MB-151) purchased from the Metal Bellows Co. is connected parallel to the driver section via half-inch stainless steel piping and two brass Hoke needle valves. Stirring of the gas-vapor mixture in the driver tube is achieved by circulation through the metal bellows pump which has a rated maximum flow rate of 1.4 S.C.F.M.

Light Scattering Equipment

Two different lasers were used as the light source. For the first set of experiments on water, heavy water and benzene, a Liconix Model 401 15mW Helium-Cadmium laser (λ = 4416 Å) was used. In the later experiments on carbon tetrachloride and freon-11, a Spectra Physics Model 124B 15mW Helium-Neon laser (λ = 6328 Å) was used because the Liconix laser had failed to emit its rated power output and needed a new plasma

tube. Two identical RCA-7265 photomultiplier tubes were used as detectors of the scattered light. This PMT is a 2-inch-diameter, 14-stage, head-on type having an S-20 spectral response which has a higher absolute sensitivity at λ = 4416 Å than at λ = 6328 Å by a factor of 2.3. Since the intensity of the scattered light in the case of Rayleigh scattering is inversely proportional to λ^4, the overall advantage in using the Helium-Cadmium laser is a tenfold increase in the light scattering signal. The current amplification factor of the PMT is 4.8×10^7. A load resistor of approximately 10 kΩ converts the anode current output to a voltage signal which is recorded on the oscillogram.

Pressure measurements

In each experiment, four different pressure measurements are made:

(i) p_{v4}, the initial partial pressure of the test vapor;

(ii) p_4, the initial total pressure in the driver section;

(iii) p_k, the total pressure at onset;

(iv) p_1, the initial pressure in the driven section.

Except for p_1 which is varied stepwise to achieve the desired expansion strength, the other three pressures are measured as accurately as possible.

In the experiments on water, heavy water and benzene, p_{v4} is measured with a calibrated Statham PM6TC ±4 psid differential pressure transducer which is connected to the driver tube via a brass Hoke needle valve. A reference pressure for the transducer is supplied by a Wallace and Tiernan Aneroid

Model FA 149 manostat connected to a vacuum pump. The reference pressure which is read with a precision Wallace and Tiernan Model FA 187 mercury manometer is set between 1 - 5 torr and is found to remain within ±0.1 torr of the set value. A Lambda Model LCS-2-02 power supply provides a 10V DC input for the transducer. The transducer output in millivolts is read on a Hewlett-Packard Model 3465A digital voltmeter (4½ digits). The experimental uncertainty in p_{v4} measured in this manner is ±0.2 torr.

In the experiments on carbon tetrachloride and Freon-11, p_{v4} is measured with an MKS Baratron head sensor (Type 310 BHS-1000) in conjunction with an indicator meter (Type 170M-6B). The voltage output from the indicator meter is read with the above mentioned HP digital voltmeter. This factory calibrated precision capacitance manometer provides a convenient measurement of p_{v4} with an experimental uncertainty of ±0.2 torr.

p_4 is measured with another calibrated Statham Model PM822 ±25 psid differential pressure transducer in a manner similar to the measurement of p_{v4} with the Statham ±4 psid pressure transducer as described above. The reference pressure in this case is provided by the atmospheric pressure which is read with another precision Wallace and Tiernan mercury manometer.

The static pressure is measured at each observation station with a Kistler pressure transducer in conjunction with a charge/voltage amplifier as described in Chapter 3. The

voltage output from the amplifier is recorded on the vertical axis of the oscillogram. p_k is the value on the pressure trace which corresponds to the moment when the light scattering signal is first observed. The onset conditions (p_{vk}, T_k) are calculated from this measured value of p_k and the initial conditions as described in Chapter 5. Calibration of the Kistler transducers is carried out by supplying known amounts of pressure change to the transducers and measuring the resulting voltage outputs on the oscillogram. In order to do this, the driven section is first separated from the driver section. A diaphragm is clamped tightly between the open end of the driver section and a brass ring. The driver tube is next filled with argon gas to a known pressure. On equalizing this pressure with the atmospheric pressure by rupturing the diaphragm, a known pressure change is applied to the Kistler transducers. The readability on a typical oscillogram is ±10 torr. This is the worst source of experimental uncertainty in the whole experiment and gives rise to an uncertainty of ±1.0 °C in the onset temperature measured.

p_1 is measured with a Wallace and Tiernan Model F160 absolute pressure gauge with a range of 0 - 800 torr. The readability on this dial gauge is ±1 torr.

Temperature measurements

The initial temperature, T_4, in the driver tube is measured by a copper-constantan thermocouple inserted into the driver tube such that its sensing tip is flush with the inner tube wall. A reference thermocouple is placed in an

ice bath. The temperature of the ice bath is measured with a precision thermometer with an accuracy of ±0.05 °C. The voltage (in microvolts) across the two thermocouples is read with a Keithley Model 160 digital voltmeter (3½ digits). The thermocouples used are calibrated together in order to find the temperature difference as a function of voltage. The experimental error in T_4 measured in this manner is ±0.1 °C.

APPENDIX 5. Nomenclature

a	local sound speed (= $\sqrt{\gamma RT/\mu}$)
c	local wave velocity (= x/t)
C_p	molar heat capacity at constant pressure
C_v	molar heat capacity at constant volume
d	hydraulic diameter; also width of window of PMT housing and width of observation window in shock tube
D	shock tube diameter; also diffusion coefficient
g	mass fraction of the condensate
I	intensity of scattered radiation at 90°
I_o	intensity of incident radiation
J	nucleation rate
k	Boltzman's constant
K	= (γ+1)/2(γ-1)
Kn	Knudsen number (= $\bar{l}$/r)
$\bar{l}$	mean free path of the gas mixture
L	latent heat
m	molecular mass; also refractive index of scatterer
n_D	refractive index for sodium light
N	number density; also dimensionless characteristic slope
p	pressure
Pr	Prandtl number (= $\eta C_p/\lambda$)
r	droplet radius
R	universal gas constant; also distance between PMT window and laser beam
Re	Reynolds number (= ρud/η)
R_L	load resistor of PMT

S	supersaturation or saturation ratio (= p_v/p_∞); also distance between PMT window and observation window of shock tube
t	time
T	temperature
u	local flow velocity
V	voltage
x	the abscissa in the x-t diagram
y	mole fraction of the condensing vapor
α	mass accommodation coefficient
α'	effective condensation coefficient that formally accounts for evaporation
γ	ratio of the specific heats
Γ	empirical adjustment factor defined in Eq.(6.6)
η	viscosity
θ	Gyarmathy's correction factor defined in Eq.(6.3)
λ	wavelength; also thermal conductivity
μ	molecular weight
ξ	thermal accommodation coefficient
ρ	density
σ	surface tension or surface energy
w	mass fraction of the condensing vapor

Subscripts

c	condensate
i	inert carrier gas
k	onset of condensation
ℓ	liquid

m	gas mixture
o	initial position of the fluid element
r	refers to a droplet of radius r; also reduced
s	solid
v	condensing vapor
cl	classical
crit	critical
exp	experimental
obs	observation station
PMT	photomultiplier tube
th	theoretical
1	condition of undisturbed driven gas; also first observation station
2	condition of driven gas traversed by the incident shock wave; also second observation station
3	condition of driver gas traversed by the incident expansion wave
4	condition of undisturbed driver gas
∞	flat-surface bulk value

Superscripts

*	refers to the critical cluster
$(\bar{\ })$	refers to mean value

LIST OF TABLES

LIST OF FIGURES

Table 5.1 Summary of Water Condensation Experiments and Results

Expt.No.	Observation Station	Initial Conditions P_4 (torr)	P_{v4} (torr)	T_4 (K)	w_4	P_{vk} (torr)	Onset Conditions T_k (K)	S_k solid	S_k liquid	$T_k - T_{mp}$ (°C)
67	1	1216.0	17.3	299.5	0.0065	11.5	254.8	12.6	10.6	-18.4
	2					11.7	256.1	11.3	9.6	-17.1
71	1	1345.5	10.5	297.8	0.0035	6.6	247.1	15.4	11.9	-26.1
	2					6.8	249.7	12.2	9.7	-23.5
72	1	1358.2	13.6	297.8	0.0045	8.9	251.6	13.3	10.6	-21.6
	2					9.0	252.2	12.7	10.3	-21.0
73	1	1370.9	12.2	297.9	0.0040	7.6	249.0	15.0	11.9	-24.2
	2					7.9	250.4	13.2	10.6	-22.8
77	1	1392.0	8.8	298.4	0.0029	5.3	244.2	16.6	12.5	-29.0
	2					5.3	244.2	16.6	12.5	-29.0
78	1	1398.2	7.1	298.3	0.0023	4.3	241.5	17.8	13.1	-31.7
	2					4.2	242.3	16.0	11.8	-30.9
80	1	1407.2	5.4	298.0	0.0017	3.0	234.7	26.1	17.7	-38.5
	2					3.1	237.6	19.6	13.6	-35.6
82	1	1454.8	3.8	298.0	0.0012	2.0	229.6	31.1	20.0	-43.6
	2					2.0	230.4	28.4	18.6	-42.8
98	1	1414.6	15.5	298.1	0.0050	10.3	252.9	13.5	11.2	-20.3
	2					10.3	252.9	13.5	11.2	-20.3

Table 5.2 Summary of Heavy Water Condensation Experiments and Results

Expt.No.	Observation Station	Initial Conditions P_4 (torr)	P_{v4} (torr)	T_k (K)	ω_4	P_{vk} (torr)	Onset T_k (K)	S_k solid	S_k liquid	$T_k - T_{mp}$ (°C)
10	1	1399.7	17.3	298.5	0.0062	12.0	257.8	13.4	10.8	-19.2
	2					12.2	259.6	11.6	9.5	-17.5
14	1	1401.7	15.6	298.0	0.0056	10.8	257.3	12.6	10.1	-19.6
	2					11.0	258.8	11.1	9.1	-18.2
19	1	1437.1	13.8	298.4	0.0048	9.1	253.0	16.2	12.5	-24.0
	2					9.2	253.7	15.3	11.8	-23.3
24	1	1421.6	12.2	298.6	0.0043	7.7	248.8	21.0	15.5	-28.2
	2					7.9	251.2	16.8	12.7	-25.6
44	1	807.5	9.7	297.3	0.0061	6.0	244.8	24.8	17.5	-32.2
	2					6.2	248.2	18.0	13.1	-28.8
48	1	804.5	8.0	297.4	0.0050	4.8	241.6	28.0	19.0	-35.4
	2					4.8	243.4	23.1	16.2	-33.6
54	1	797.1	6.3	297.4	0.0040	3.6	237.6	32.8	21.4	-39.3
	2					3.7	239.5	27.2	18.1	-37.5
55	1	823.7	4.6	297.5	0.0028	2.5	234.1	34.0	21.7	-42.8
	2					2.6	235.2	31.1	19.6	-41.7
57	1	822.9	2.9	297.5	0.0018	1.5	228.0	42.2	25.0	-49.0
	2					1.5	229.2	36.5	22.2	-47.8
59	1	857.3	1.6	297.5	0.0009	0.7	217.4	77.0	43.1	-59.6
	2					0.8	219.2	69.2	35.4	-57.8

Table 5.3 Summary of Benzene Condensation Experiments and Results

Expt.No.	Observation Station	Initial Conditions P_4 (torr)	P_{v4} (torr)	T_4 (K)	y_4	P_{vk} (torr)	Onset T_k (K)	S_k solid	S_k liquid	$T_k - T_{mp}$ (°C)
20	1	1055.2	84.2	296.4	0.0798	37.7	228.4	74.3	26.9	-50.3
	2					39.4	231.7	55.6	21.8	-47.0
21	1	1099.6	73.6	296.4	0.0669	31.2	222.4	114.5	36.2	-56.3
	2					32.5	225.5	86.1	29.2	-53.2
22	1	1090.5	78.7	296.4	0.0722	34.6	226.0	87.0	29.9	-52.7
	2					34.8	226.4	84.0	29.1	-52.3
23	1	1054.7	82.0	296.1	0.0778	34.9	224.1	107.0	35.2	-54.6
	2					35.8	226.0	90.1	30.9	-52.7
24	1	1018.3	77.8	296.0	0.0764	32.7	223.1	111.4	35.8	-55.6
	2					33.4	224.7	96.2	32.1	-54.0
25	1	1053.2	73.5	296.0	0.0698	30.6	221.1	129.1	39.6	-57.6
	2					31.3	223.0	107.8	34.5	-55.7
26	1	1090.2	63.9	296.0	0.0586	26.5	219.2	137.3	40.2	-59.5
	2					26.9	220.4	122.4	36.9	-58.3
27	1	1091.6	60.8	296.0	0.0557	24.3	215.8	183.5	49.6	-62.9
	2					25.1	218.4	142.0	40.8	-60.3
38	1	1353.9	31.6	296.6	0.0233	11.9	205.6	297.3	62.5	-73.1
	2					12.4	209.0	205.5	47.0	-69.7
39	1	1357.8	40.6	296.7	0.0299	15.6	208.4	277.7	62.6	-70.3
	2					16.7	214.0	154.6	40.0	-64.7

Table 5.4 Summary of Carbon Tetrachloride Condensation Experiments and Results

Expt.No.	Observation Station	Initial Conditions P_4 (torr)	P_{v4} (torr)	T_4 (K)	y_4	Onset Conditions P_{vk} (torr)	T_k (K)	S_k solid	S_k liquid	$T_k - T_{mp}$ (°C)
100	1	1867.3	53.9	296.8	0.0286	24.7	222.3	28.7	26.1	-28.2
	2					24.9	223.0	27.1	24.7	-27.5
103	1	1988.8	78.1	297.2	0.0393	36.2	225.4	31.7	29.1	-25.1
	2					36.5	226.1	30.0	27.6	-24.4
104	1	2012.6	64.1	297.2	0.0319	29.7	224.2	29.0	26.5	-26.3
	2					29.9	224.7	27.9	25.5	-25.8
106	1	2084.0	44.2	297.5	0.0212	18.6	214.6	45.0	40.8	-35.9
	2					18.7	215.0	43.5	39.4	-35.5
108	1	2000.2	37.6	297.7	0.0188	15.6	213.0	44.2	40.2	-37.5
	2					15.7	213.5	42.4	38.4	-37.0
110	1	2002.8	28.2	297.8	0.0141	11.2	208.3	51.4	47.0	-42.2
	2					11.3	209.6	45.3	41.3	-40.9
111	1	2004.1	65.0	297.8	0.0324	28.7	220.9	37.9	34.5	-29.6
	2					29.2	222.2	34.2	31.2	-28.3
113	2	2043.9	90.4	299.2	0.0442	43.3	230.5	24.3	22.5	-20.0
118	2	2091.9	104.0	298.4	0.0497	49.8	230.8	27.2	25.3	-19.7

Table 5.5 Summary of Freon-11 Condensation Experiments and Results

Expt.No.	Observation Station	Initial Conditions P_4 (torr)	P_{v4} (torr)	T_4 (K)	y_4	Onset Conditions P_{vk} (torr)	T_k (K)	S_k liquid	$T_k - T_{mp}$ (°C)
16	1	2097.5	400.6	290.8	0.1910	149.3	222.3	7.89	+60.3
	2					156.9	225.3	6.75	+63.3
17	1	2080.9	407.4	289.3	0.1958	153.6	222.4	8.10	+60.4
	2					160.5	225.0	7.07	+63.0
22	1	2108.2	311.5	288.2	0.1478	124.4	220.2	7.65	+58.2
	2					129.1	222.6	6.71	+60.6
60	2	2259.9	121.4	286.5	0.0537	49.1	208.0	7.62	+46.0
67	2	2154.2	146.1	285.8	0.0678	59.8	210.4	7.66	+48.4
70	2	2138.0	185.7	284.8	0.0869	78.9	214.7	7.23	+52.7
83	2	2041.9	102.5	284.5	0.0502	41.6	204.3	8.48	+42.3
84	2	2369.7	82.0	284.8	0.0346	32.1	201.4	8.69	+39.4

Table 6.1 Summary of comparison of results with theory.

Exp.No.(Obs.St.No.)	Initial Conditions			Experimental Onset Conditions					Calculated Onset Values							
	P_d (torr)	T_d (K)	P_{vd} (torr)	P_{vk} (torr)	T_k (K)	$T_k - T_{sp}$ (K)	$\log(p_v/p_\infty)_k$ solid	liquid	$\log r$ solid	liquid	r_k^* (Å) solid	liquid	n_k (cm^{-3}) solid	liquid	$\bar{r}_k$ (Å) solid	liquid
Water (H_2O) in argon																
71(1)	1346	298	10.5	6.6	247	-26	15.4	11.9	12	4	6.4	5.8	3.8×10^{11}	1.5×10^{10}	139	263
71(2)				6.8	250	-23	12.2	9.7	12	4	6.8	5.9	1.3×10^{11}	2.5×10^{10}	192	296
73(1)	1371	298	12.2	7.8	249	-24	15.0	11.9	12	3	6.5	5.5	2.5×10^{11}	7.9×10^{9}	138	235
73(2)				7.9	250	-23	13.2	10.6	14	4	6.9	6.0	8.1×10^{9}	3.9×10^{9}	183	359
77(1)	1392	298	8.8	5.3	244	-29	16.6	12.5	14	5	6.7	5.8	8.3×10^{11}	1.6×10^{10}	116	163
77(2)				5.3	244	-29	16.6	12.5	14	5	6.8	6.0	1.2×10^{11}	4.5×10^{9}	159	268
Heavy Water (D_2O) in argon																
24(1)	1422	299	12.2	7.7	249	-28	21.0	15.5	8	1	5.9	5.2	1.6×10^{11}	4.8×10^{9}	169	273
24(2)				7.9	251	-26	16.8	12.7	10	2	6.4	5.6	6.5×10^{9}	2.7×10^{9}	233	411
44(1)	808	297	9.7	6.0	245	-32	24.8	17.5	8	2	5.8	5.3	2.9×10^{11}	1.2×10^{10}	155	248
44(2)				6.2	248	-29	18.9	13.1	8	2	6.0	5.5	4.0×10^{9}	3.7×10^{9}	217	396
48(1)	805	297	8.0	4.8	242	-35	28.0	19.0	8	2	5.7	5.2	2.7×10^{11}	5.0×10^{9}	129	182
48(2)				4.8	243	-34	23.1	16.2	8	3	5.9	5.6	3.3×10^{9}	5.4×10^{9}	185	322
Benzene (C_6H_6) in argon																
25(1)	1053	296	73.5	30.6	221	-58	129.1	39.6	3	7	8.2	10.0	6.4×10^{7}	1.5×10^{7}	1320	1520
25(2)				31.3	223	-56	107.8	34.5	3	7	8.3	10.1	4.5×10^{7}	1.2×10^{7}	1870	2150
27(1)	1092	296	60.8	24.3	216	-63	183.5	49.6	1	7	7.7	9.6	1.9×10^{7}	3.4×10^{7}	1430	1500
27(2)				25.1	218	-60	142.0	40.8	2	8	8.1	10.0	1.5×10^{7}	2.8×10^{7}	1920	2040
Carbon Tetrachloride (CCl_4) in argon																
103(1)	1989	297	78.1	36.2	225	-25	31.7	29.1	3	6	9.1	9.7	2.5×10^{7}	5.6×10^{7}	1680	1920
103(2)				36.5	226	-24	30.0	27.6	4	6	9.4	10.0	3.3×10^{7}	1.1×10^{7}	2110	2420
111(1)	2004	298	65.0	28.7	221	-29	37.9	34.5	2	5	8.7	9.4	1.9×10^{7}	9.2×10^{6}	1860	1990
111(2)				29.2	222	-28	34.2	31.2	3	6	9.2	9.9	7.0×10^{6}	4.9×10^{6}	2170	2370
113(2)	2044	299	90.4	43.3	230	-20	24.3	22.5	4	6	9.8	10.3	3.2×10^{6}	4.6×10^{6}	2080	2480
118(2)	2092	298	104.0	49.8	231	-19	27.2	25.3	3	4	9.3	9.8	2.1×10^{6}	4.9×10^{6}	2400	2890
Freon-11 (CCl_3F) in argon																
16(1)	2098	291	400.6	149.3	222	+60	-	7.9	-	11	-	7.4	-	2.3×10^{7}	-	2430
16(2)				156.9	225	+63	-	6.8	-	12	-	6.6	-	6.3×10^{6}	-	3130
17(1)	2081	289	407.4	153.6	222	+60	-	8.1	-	10	-	7.7	-	2.4×10^{7}	-	2590
17(2)				160.5	225	+63	-	7.1	-	11	-	6.9	-	1.1×10^{7}	-	3230
22(1)	2108	288	311.5	124.4	220	+58	-	7.7	-	9	-	9.2	-	5.4×10^{6}	-	2290
22(2)				129.1	223	+61	-	6.7	-	10	-	8.2	-	2.8×10^{6}	-	2900

Table 6.2 Summary of Γ-values

Substance	$\Delta T = T_k - T_{mp}$ (K)	log Γ liquid	log Γ solid	References*
H_2O	-62 to -53	4	5 to 7	(a)
H_2O	-27 to -19	3	-	(b)
H_2O	0 to +41	-3 to 1	-	(c)
H_2O	-29 to -23	3 to 5	12 to 14	This work
D_2O	-32 to -22	1 to 3	8 to 10	This work
C_6H_6	-78 to -63	8 to 9	2 to 4	(d)
C_6H_6	-73 to -47	7 to 8	1 to 3	This work
CCl_4	-45 to -30	6 to 7	-	(e)
CCl_4	-41 to -20	4 to 6	2 to 4	This work
CCl_3F	- 3 to +10	12 to 14	-	(d)
CCl_3F	+39 to +63	9 to 12	-	This work

* These Γ-values are found by Wegener and Wu (1977) for the following experiments:
(a) Pouring (1963), Wegener and Pouring (1964), Stein (1967);
(b) Barschdorff (1975);
(c) Barschdorff (1975), Binnie and Green (1943), Gyarmathy and Meyer (1965), Deych et al.(1969), Barschdorff (1971);
(d) Dawson et al.(1969);
(e) Barschdorff (1972).

Table A2.1. Onset Conditions for Water of Different Purities

Expt.No.	Quality of Water	Observation Station	P_4 (torr)	P_{v4} (torr)	T_4 (K)	Onset Conditions P_{vk} (torr)	Onset Conditions T_k (K)
75	tap	1	1403.7	15.5	298.2	10.3	253.2
		2				10.3	253.2
87	distilled	1	1394.6	15.6	298.1	10.4	253.5
		2				10.3	253.0
98	ultra-pure	1	1414.6	15.5	298.1	10.3	252.9
		2				10.3	252.9
173	tap	1	1215.0	11.0	297.3	6.9	246.6
		2				6.8	245.5
149	distilled	1	1213.0	11.0	297.0	6.8	245.5
		2				6.8	245.1
120	ultra-pure	1	1214.5	10.9	298.5	6.6	243.9
		2				6.6	244.1
167	tap	1	1222.5	8.1	297.4	4.8	242.1
		2				4.8	241.8
140	distilled	1	1228.3	8.1	297.5	4.8	241.7
		2				4.8	241.9
134	ultra-pure	1	1228.6	8.0	297.5	4.9	244.0
		2				4.8	243.3

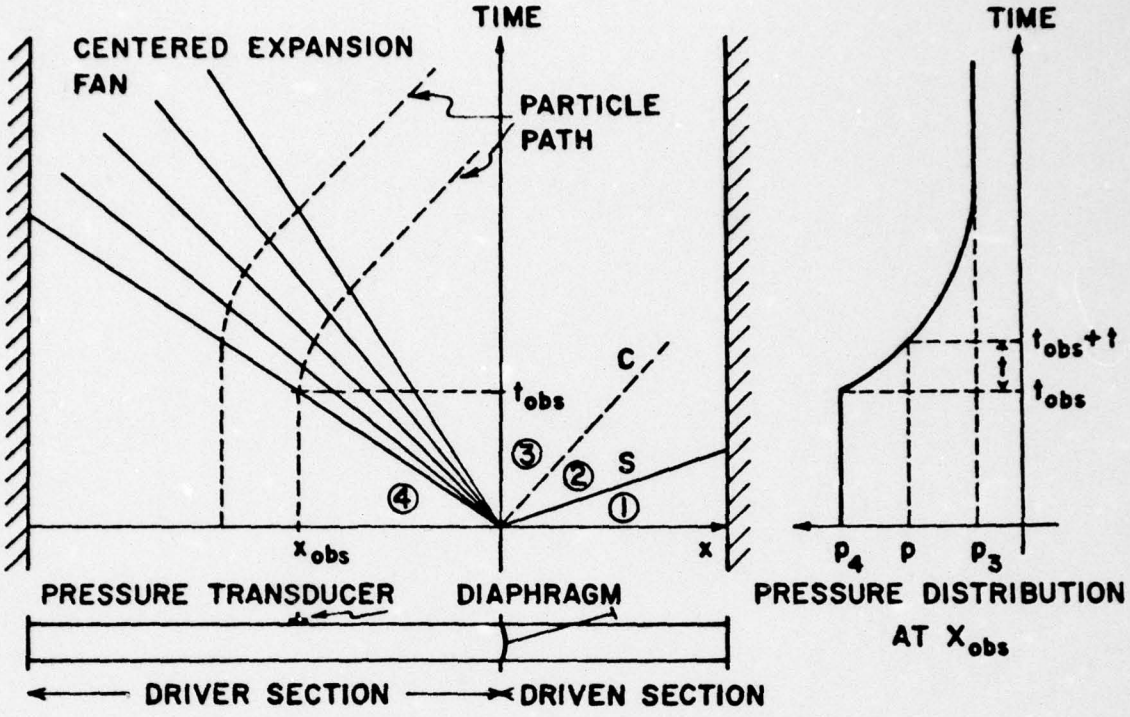

Figure 2.1 Schematic x-t diagram showing the centered expansion fan in the driver section of a shock tube.

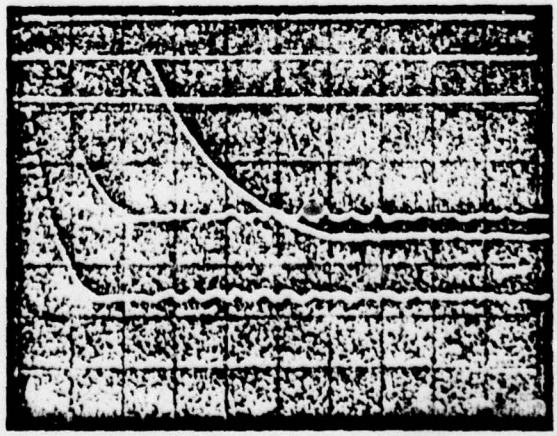

Figure 3.1 Oscilloscope traces showing experimentally measured pressure variations at three different locations situated at 127 mm, 178 mm and 495 mm respectively upstream from the diaphragm location. For the first (bottom) and second (top) stations, 99 torr/div. vertical; for the third (middle) station, 109 torr/div. vertical. The common time base is 0.5 ms/div. horizontal. The gas employed was argon. p_4 = 777.1 torr; p_4/p_1 = 3.70; $T_4 = T_1$ = 297.4 K.

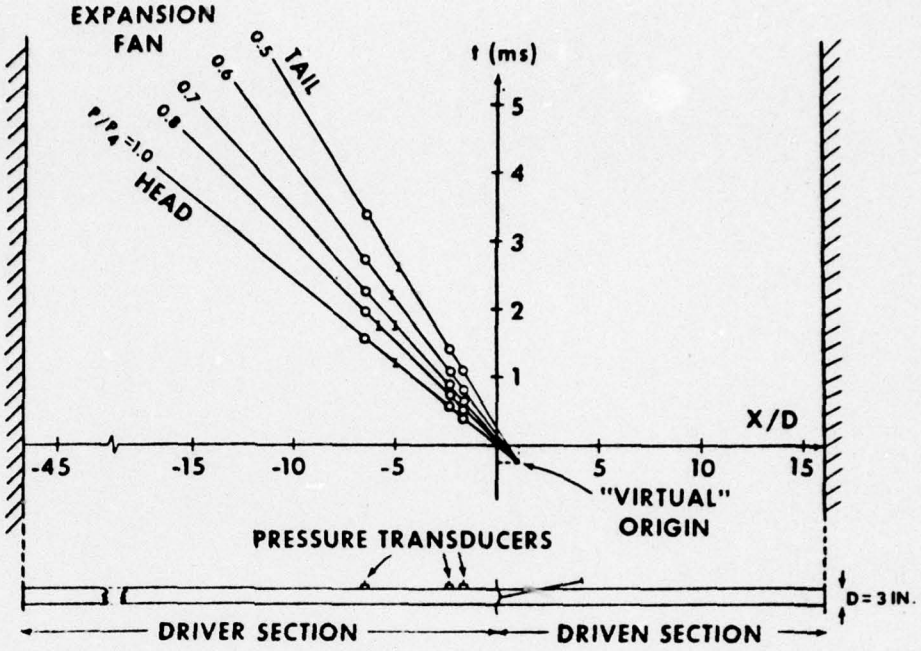

Figure 3.2 Pressure measurements of Figure 3.1 mapped into an x-t plane.

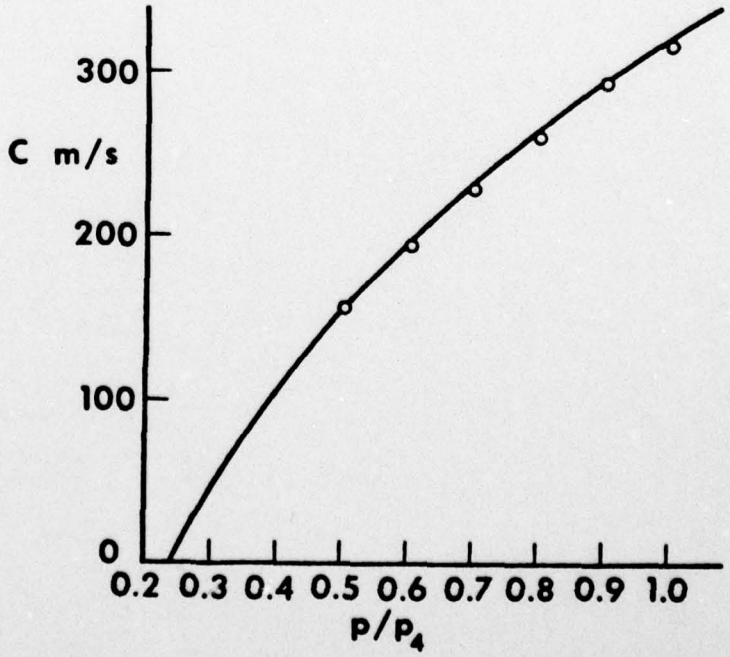

Figure 3.3 Wave speeds determined from Figure 3.2.
O Experiment; ——— Theory.

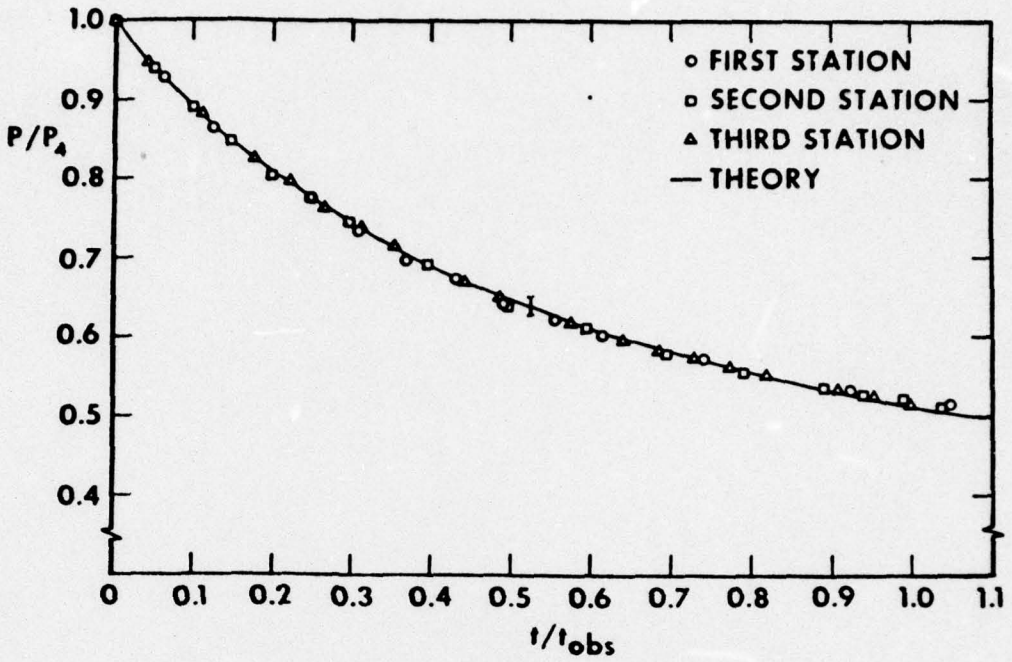

Figure 3.4 Plots of p/p_4 versus t/t_{obs} comparing the pressure measurements of three different observation stations with theory.

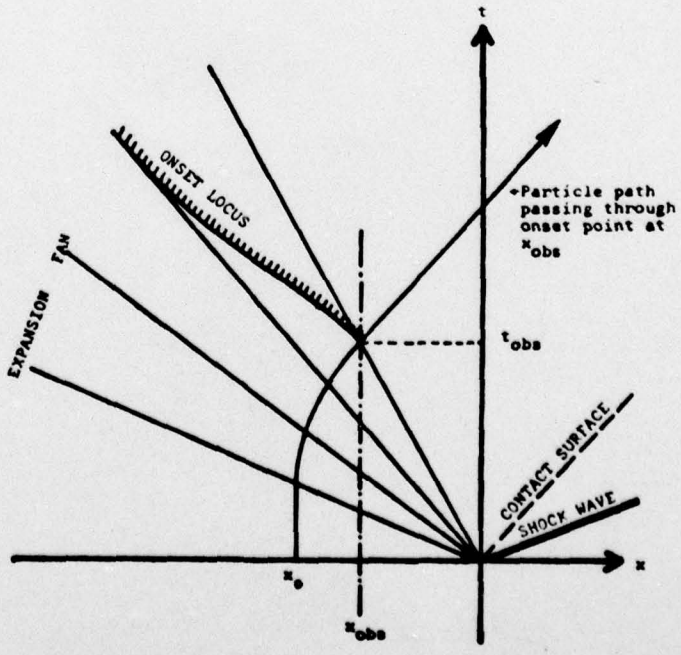

Figure 4.1 Schematic x-t diagram showing the intersection of the condensation onset locus with the tail of the expansion fan.

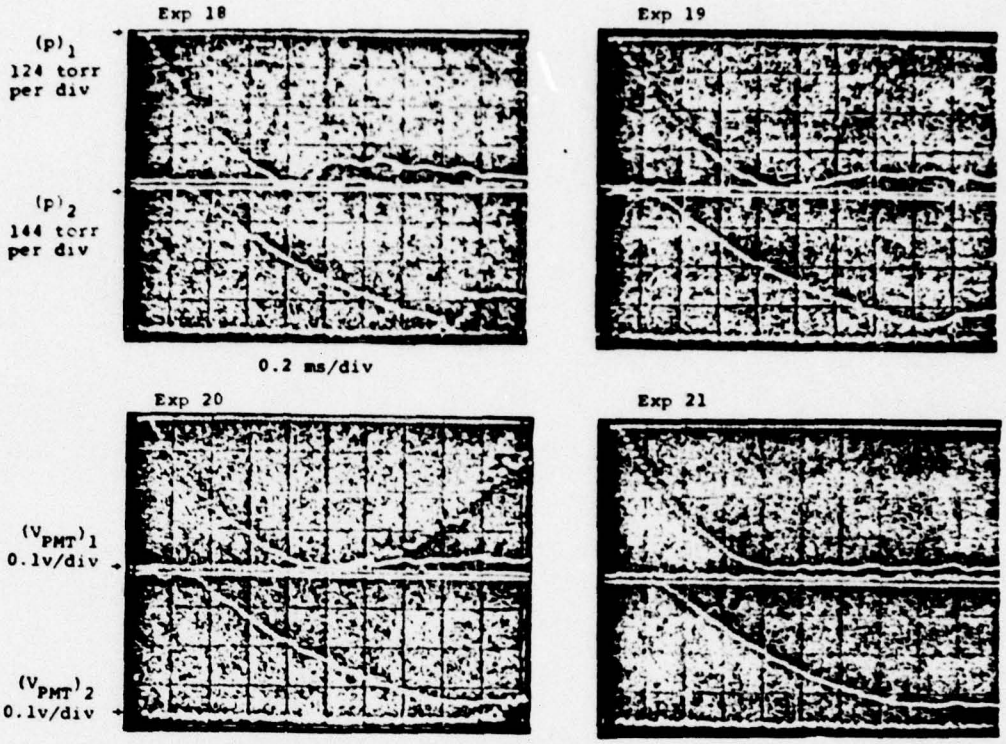

Figure 4.2 A sequence of four experiments on heavy water in argon showing how onset of condensation is determined.

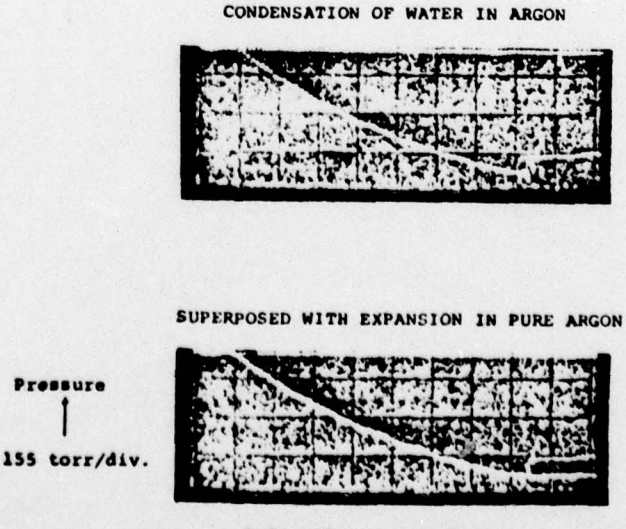

Figure 4.3 Oscillograms showing isentropic flow in the expansion wave is preserved in a condensation experiment up to the point of condensation onset.

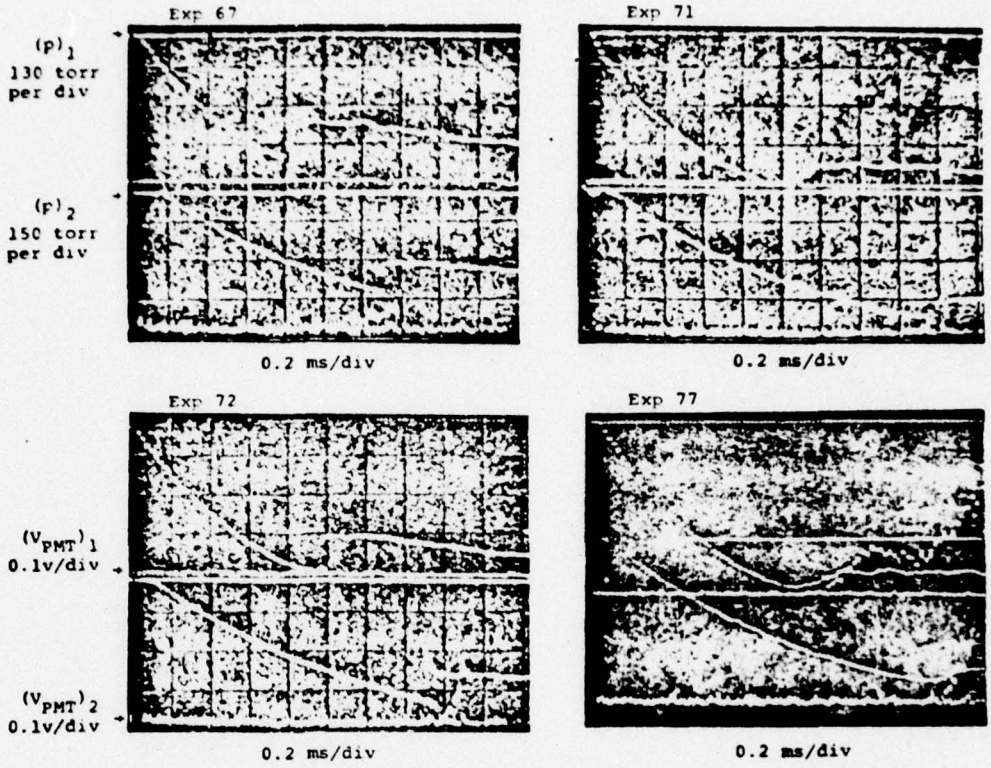

Figure 5.1 Selected oscillograms from water condensation experiments.

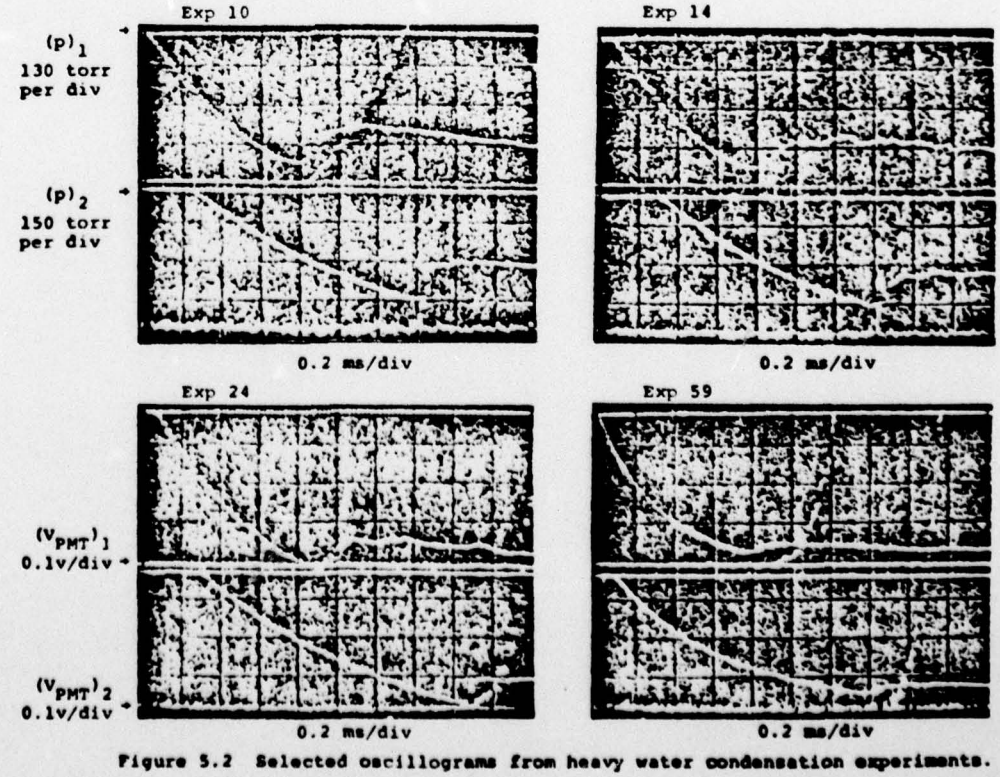

Figure 5.2 Selected oscillograms from heavy water condensation experiments.

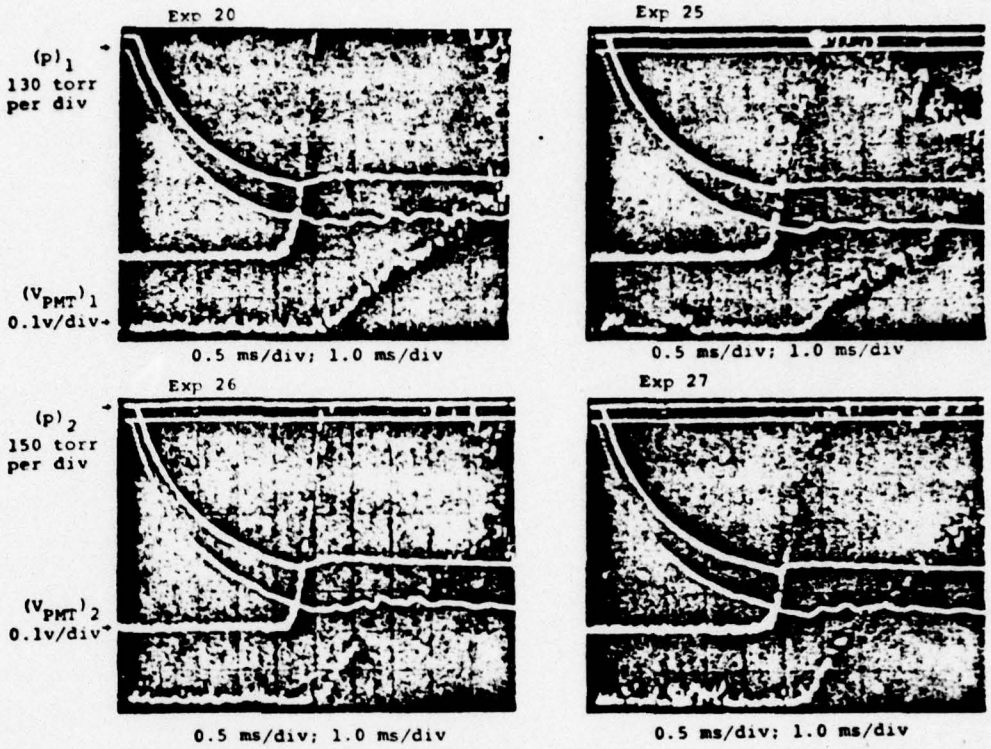

Figure 5.3 Selected oscillograms from benzene condensation experiments.

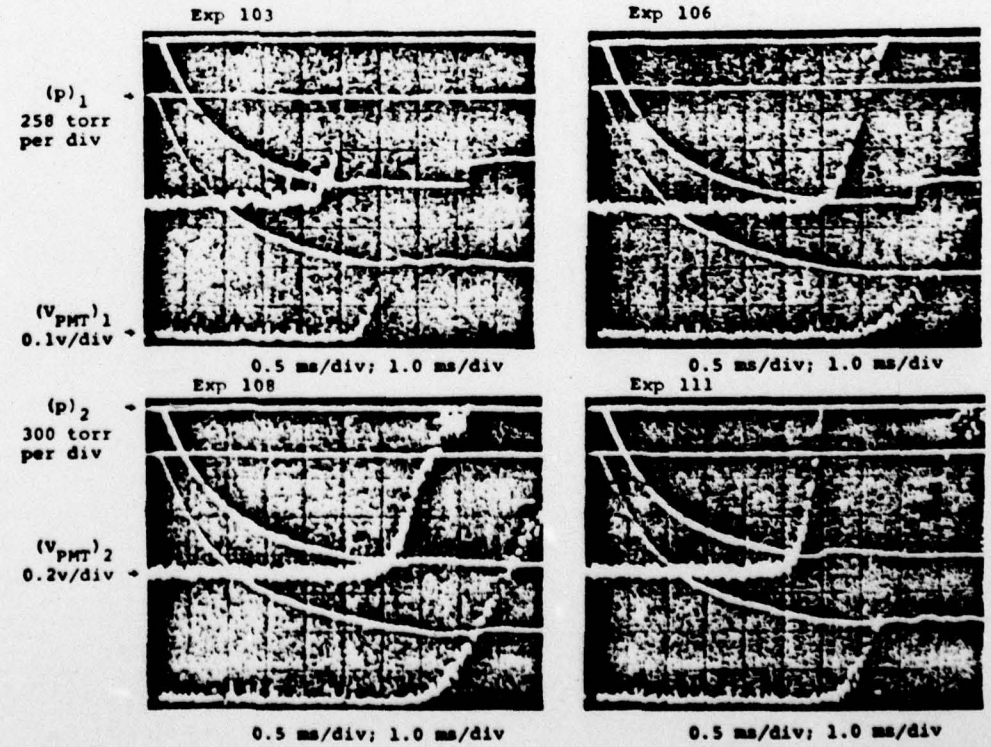

Figure 5.4 Selected oscillograms from carbon tetrachloride condensation experiments.

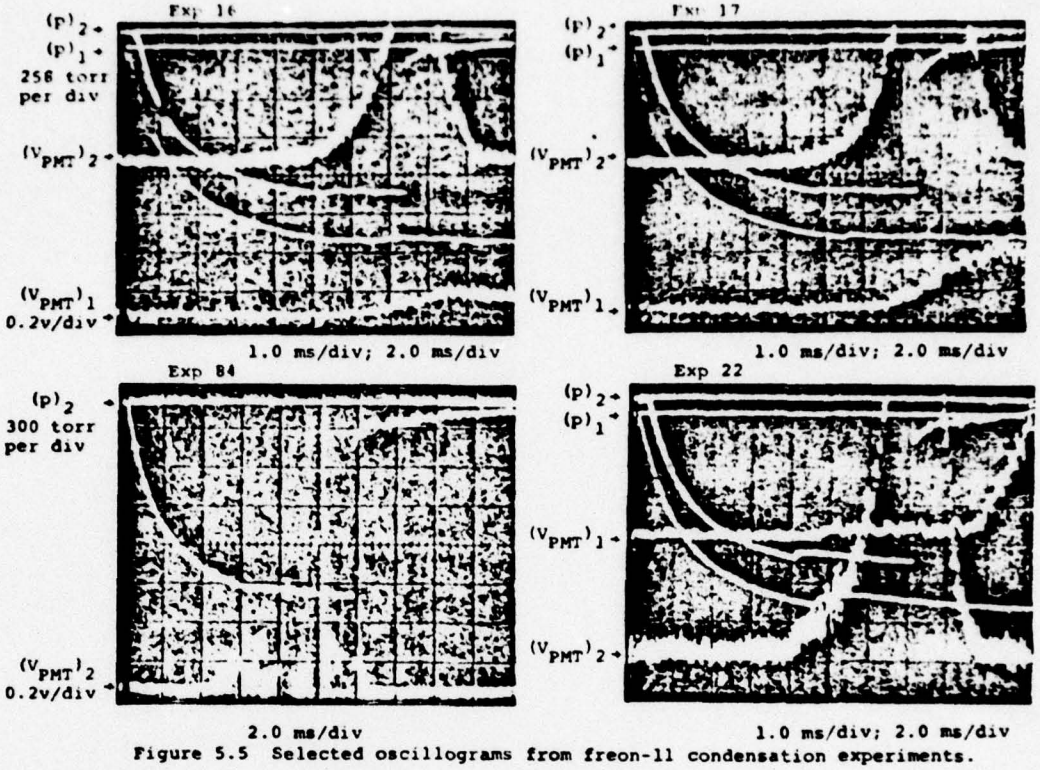

Figure 5.5 Selected oscillograms from freon-11 condensation experiments.

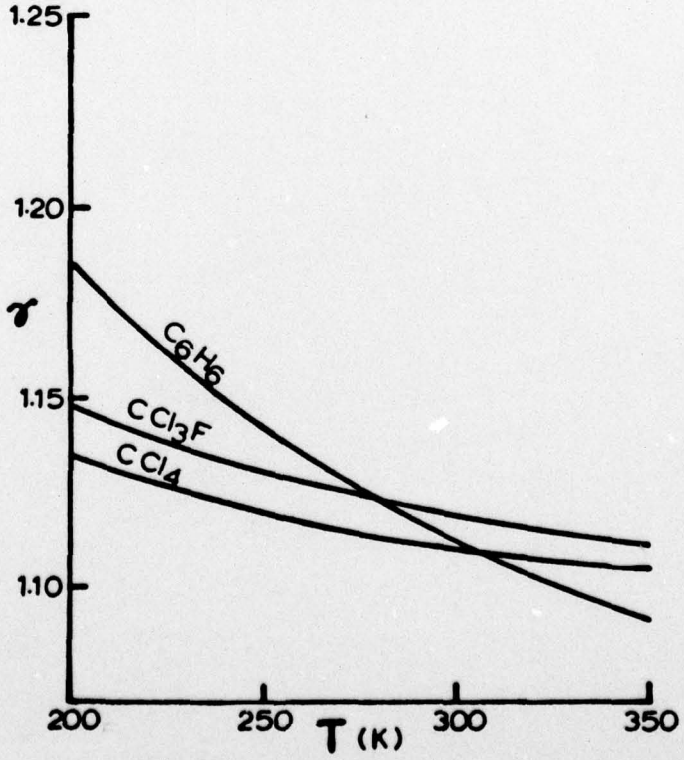

Figure 5.6 Variation of γ with temperature for benzene, carbon tetrachloride and freon-11.

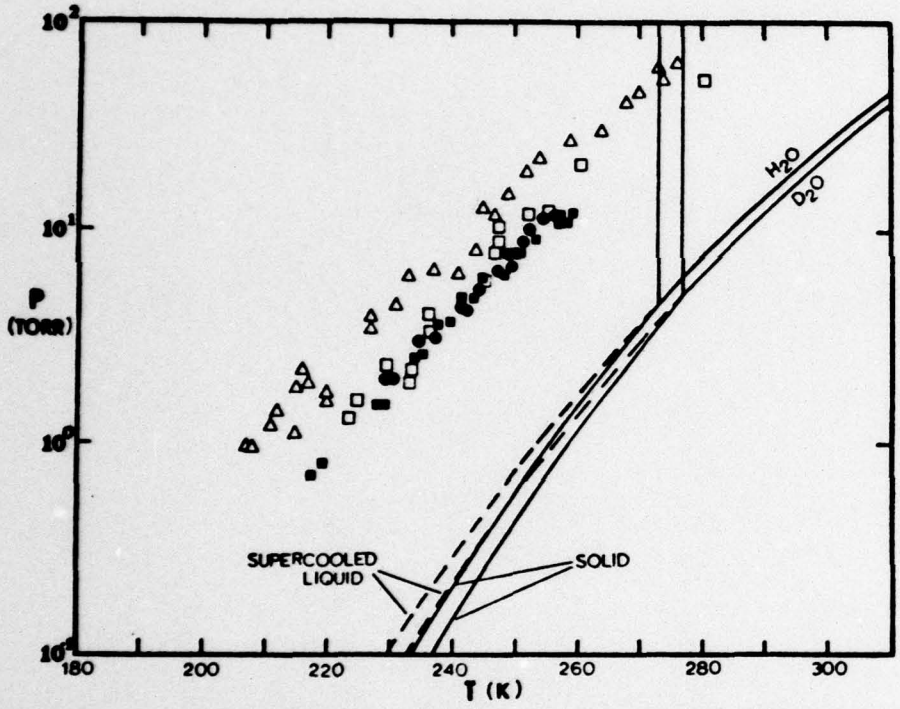

Figure 5.7 Onset conditions for the condensation of water and heavy water △ H_2O: Pouring(1963), Stein(1967) and Roberts(1969); □ H_2O: Barschdorff(1975); ● H_2O: This work. ■ D_2O: This work.

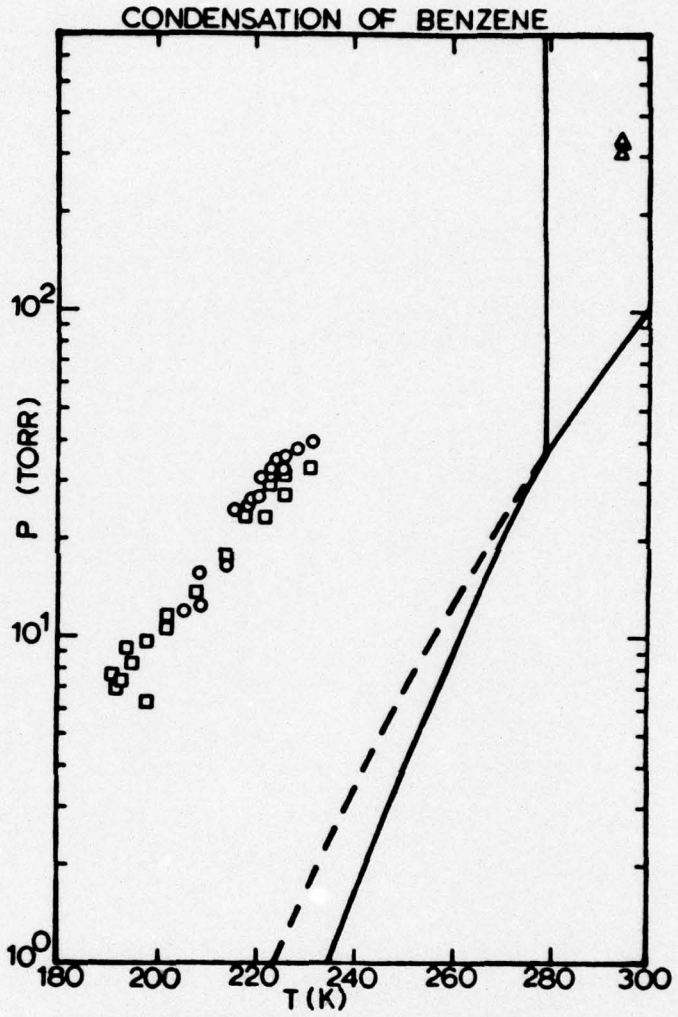

Figure 5.8 Onset conditions for the condensation of benzene. △ Katz et al.(1976); □ Dawson et al.(1969); ○ This work.

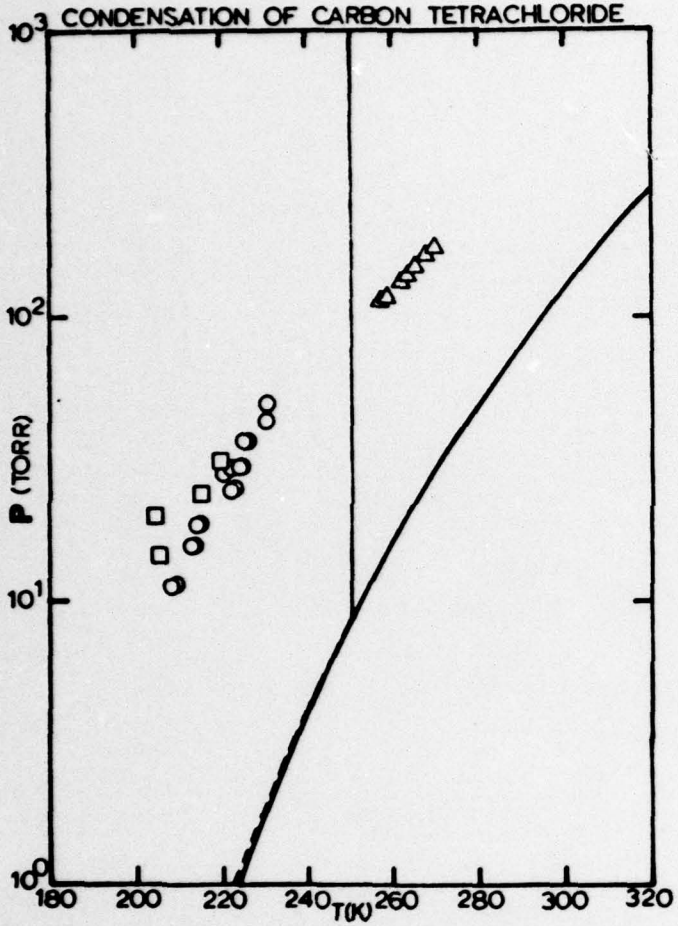

Figure 5.9 Onset conditions for the condensation of carbon tetrachloride. △ Katz et al.(1976); □ Barschdorff(1974); ○ This work.

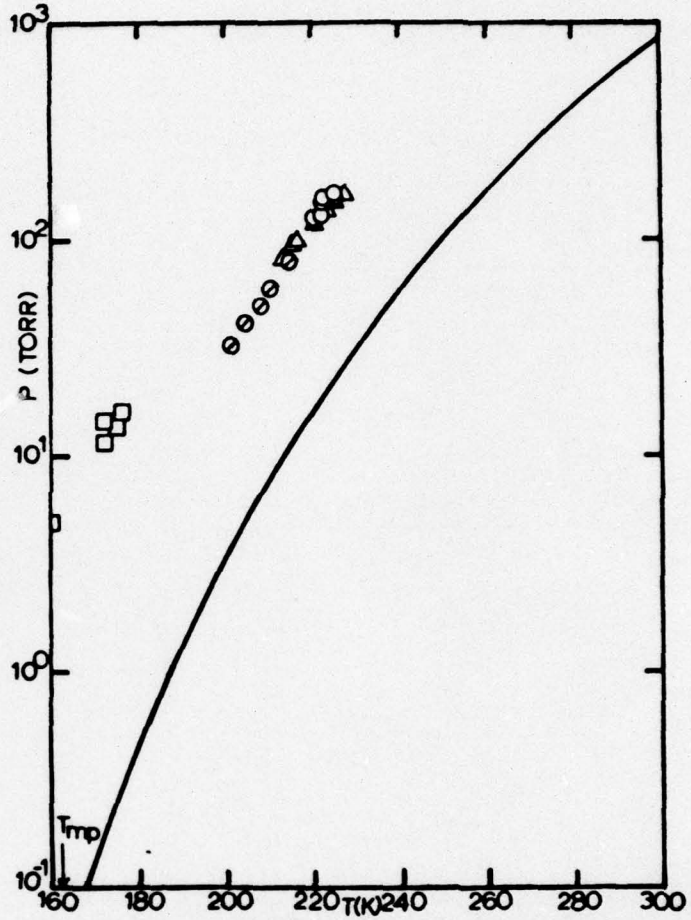

Figure 5.10 Onset conditions for the condensation of freon-11. △ Katz et al.(1976); □ Dawson et al.(1969); ⊘ This work(pressure deviation); ○ This work (light scattering).

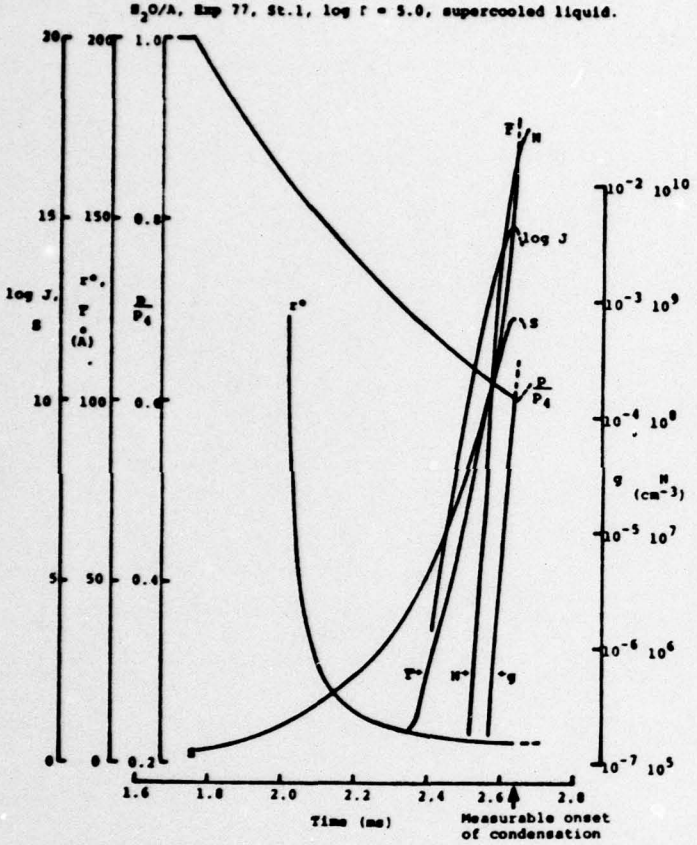

Figure 6.1 Calculated profiles along a particle path in a water condensation experiment.

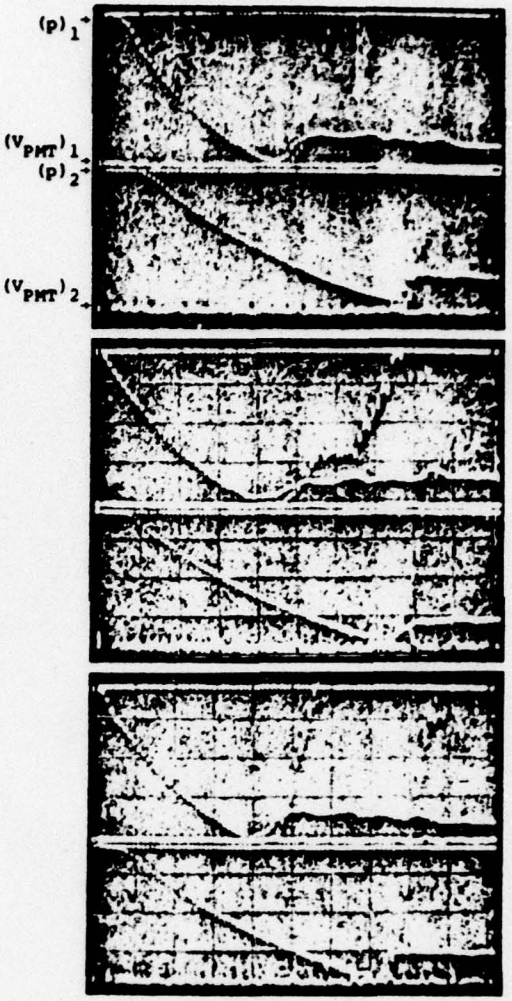

Exp 75 Tap Water in Argon

P_{v4} = 15.5 torr
P_4 = 1403.7 torr
T_4 = 298.2 K
w_4 = 0.0050

Exp 87 Distilled Water in Argon

P_{v4} = 15.6 torr
P_4 = 1394.6 torr
T_4 = 298.1 K
w_4 = 0.0051

Exp 98 Ultra-Pure Reagent Water in Argon

P_{v4} = 15.5 torr
P_4 = 1414.6 torr
T_4 = 298.1 K
w_4 = 0.0050

Scale: 124 torr/div. for $(p)_1$; 144 torr/div. for $(p)_2$;
0.1 v/div. for $(V_{PMT})_1$ and $(V_{PMT})_2$;
0.2 ms/div. for the common time base.

Figure A2.1 Oscillograms for water of three different purities.

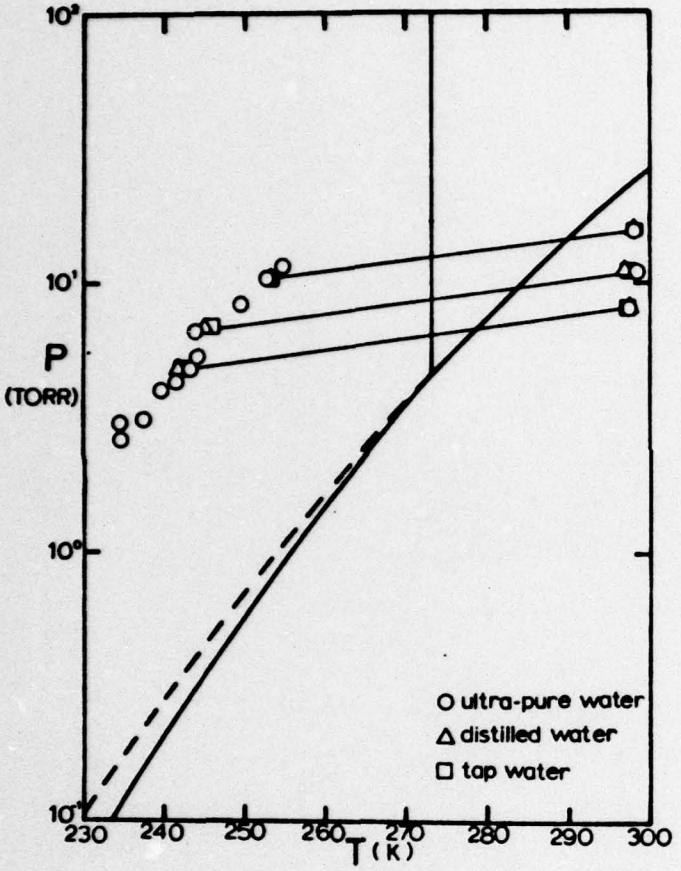

Figure A2.2 Condensation onset data showing the effect of the purity of water on the condensation of water.

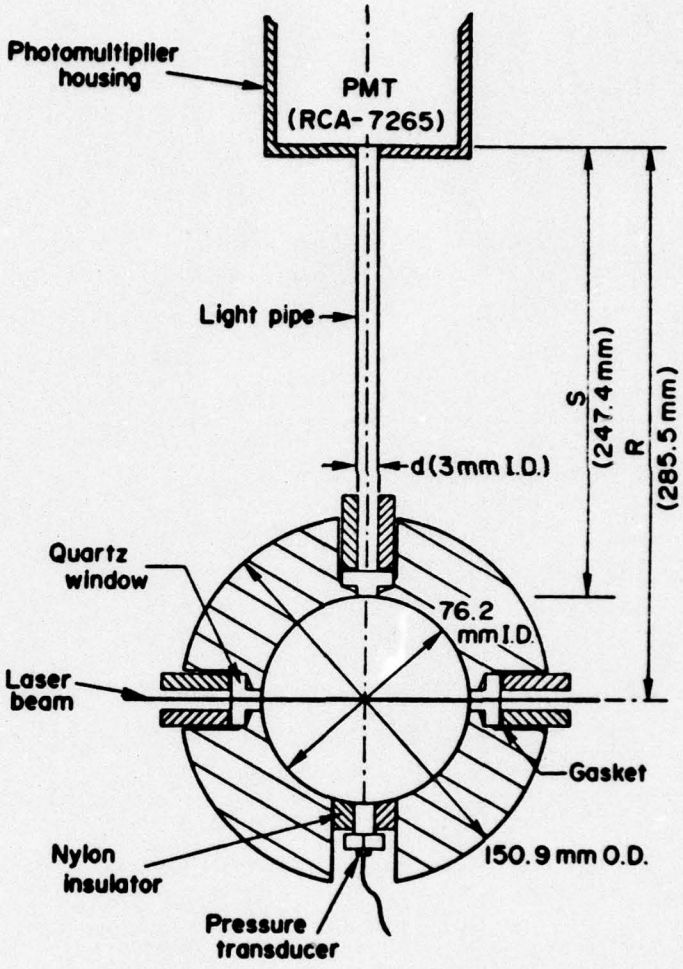

Figure A3.1 Pressure and light scattering apparatus at the second observation station.

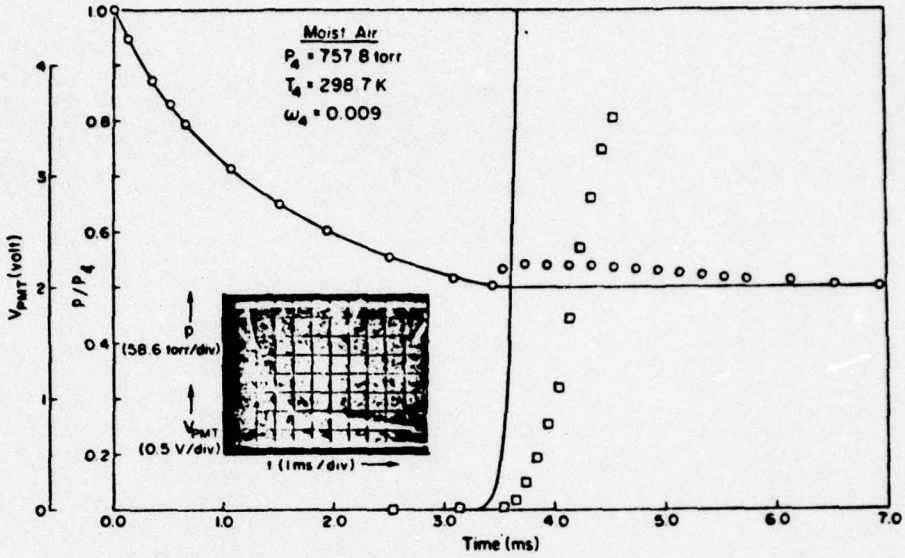

Figure A3.2 Comparison of the measured and the calculated pressure and light scattering signals.

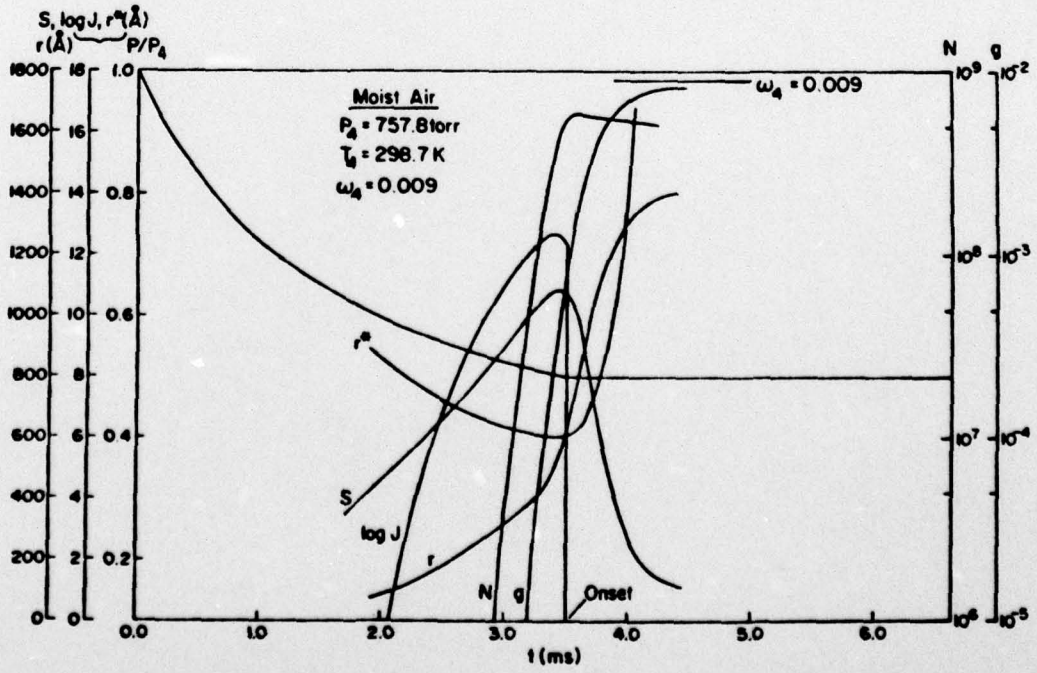

Figure A3.3 Calculated profiles for a moist air condensation experiment.

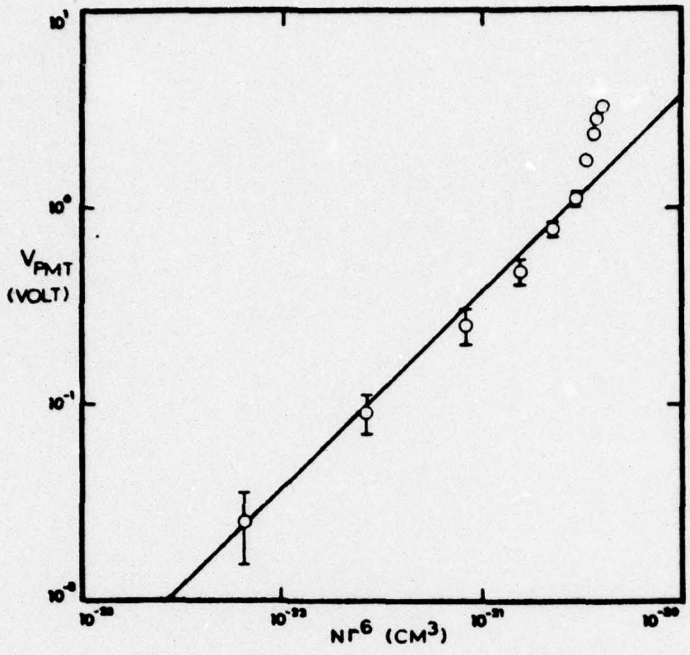

Figure A3.4 Plot of measured light scattering signal (V_{PMT}) versus calculated Nr^6.

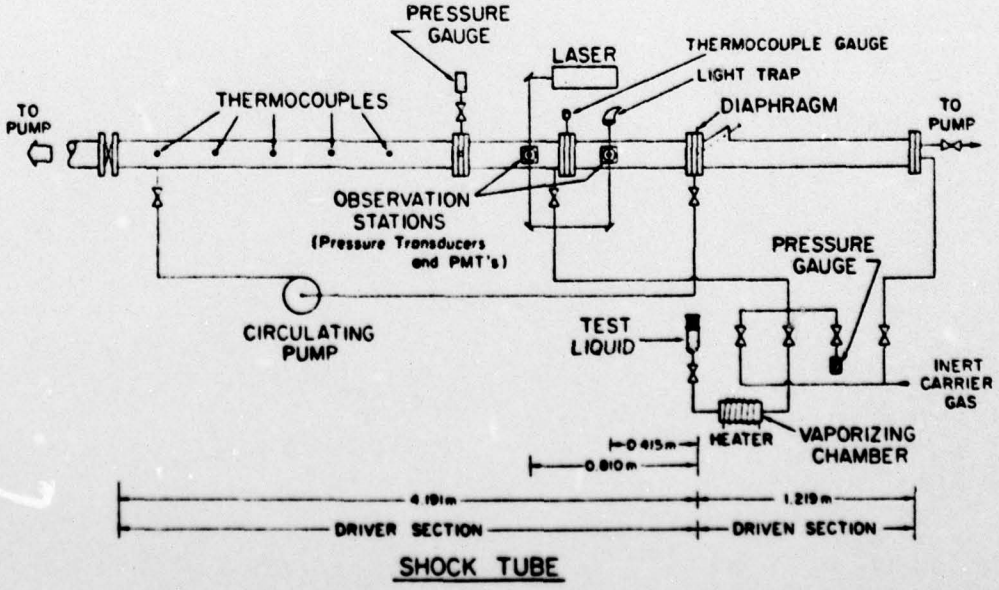

Figure A4.1 Schematic drawing of the experimental apparatus.

Unclassified

SECURITY CLASSIFICATION OF THIS PAGE (When Data Entered)

REPORT DOCUMENTATION PAGE		READ INSTRUCTIONS BEFORE COMPLETING FORM
1. REPORT NUMBER	2. GOVT ACCESSION NO.	3. RECIPIENT'S CATALOG NUMBER
4. TITLE (and Subtitle) AN EXPERIMENTAL INVESTIGATION OF THE CRITICAL SUPERSATURATION OF FIVE VAPORS IN A SHOCK TUBE		5. TYPE OF REPORT & PERIOD COVERED
		6. PERFORMING ORG. REPORT NUMBER #37
7. AUTHOR(s) C.F. Lee		8. CONTRACT OR GRANT NUMBER(s) N00014-75-C-0263
9. PERFORMING ORGANIZATION NAME AND ADDRESS Department of Engineering and Applied Science Yale University New Haven, CT 06520		10. PROGRAM ELEMENT, PROJECT, TASK AREA & WORK UNIT NUMBERS
11. CONTROLLING OFFICE NAME AND ADDRESS Power Program, Office of Naval Research Arlington, VA 22217		12. REPORT DATE January 1978
		13. NUMBER OF PAGES 66
14. MONITORING AGENCY NAME & ADDRESS (if different from Controlling Office)		15. SECURITY CLASS. (of this report) Unclassified
		15a. DECLASSIFICATION/DOWNGRADING SCHEDULE

16. DISTRIBUTION STATEMENT (of this Report)

Approved for public release, distribution unlimited.

17. DISTRIBUTION STATEMENT (of the abstract entered in Block 20, if different from Report)

18. SUPPLEMENTARY NOTES

19. KEY WORDS (Continue on reverse side if necessary and identify by block number)

Condensation, Clustering, Benzene, Water, Heavy Water, Carbon Tetrachloride, Freon 11, Nucleation, Shock Tubes.

20. ABSTRACT (Continue on reverse side if necessary and identify by block number)

Pressure measurements at three different locations in the driver section of a shock tube reveal that the expansion wave generated by diaphragm rupture can be effectively viewed as a simple centered expansion wave whose origin is slightly shifted with respect to the origin of an ideal x-t diagram. The resulting centered expansion wave is used to study the condensation of water, heavy water, benzene, carbon tetrachloride and Freon 11, in

(Continued on reverse side)

DD FORM 1 JAN 73 1473 EDITION OF 1 NOV 65 IS OBSOLETE

Unclassified

SECURITY CLASSIFICATION OF THIS PAGE (When Data Entered)

an excess of the non-condensing carrier argon. Simultaneous pressure and light scattering measurements determine the onset of condensation. The isentropic flow within the expansion wave is found to be preserved up to the point of the detectable onset of condensation by tailoring the onset conditions to occur at the tail of the expansion wave, thus rendering a simple analysis of the experiments possible.

The experimental onset of conditions of the various substances studied generally agree with previous findings in supersonic nozzles, shock tubes and diffusion cloud chambers. No difference is found in the onset of condensation of H_2O and D_2O. The homogeneous nucleation of both H_2O and D_2O is well predicted by the classical theory if it is assumed that both vapors nucleated as supercooled liquid droplets at 17-44°C and 18-49°C below their respective melting points. The homogeneous nucleation of benzene at 47-73°C below its melting point also follows the classical theory if solid condensates are assumed. Agreement with the classical theory is also found for carbon tetrachloride. The nucleation rates of Freon 11 are found to be higher than those predicted by the classical theory.